J. Fluid Mech. (2021), *vol*. 915, A88, doi:10.1017/jfm.2021.120

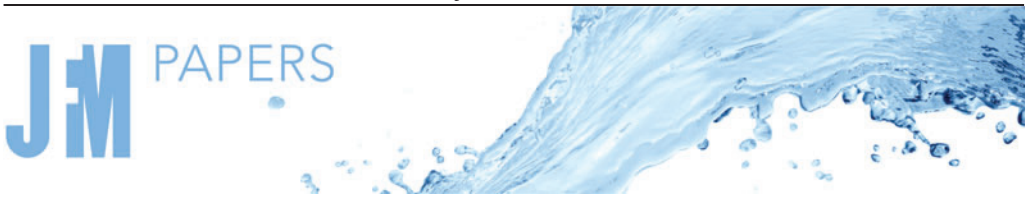

Electrohydrodynamic-induced interactions between droplets

Santanu Kumar Das[1], **Amaresh Dalal**[1] **and Gaurav Tomar**[2,†]

[1]Department of Mechanical Engineering, Indian Institute of Technology, Guwahati, India

[2]Department of Mechanical Engineering, Indian Institute of Science, Bangalore, India

(Received 7 August 2020; revised 27 November 2020; accepted 1 February 2021)

Dispersion of droplets in an emulsion is commonly seen in several chemical, pharmaceutical and petroleum industries. Electric field has been shown to affect the stability of these dispersions. We study the dynamics of a pair of leaky dielectric droplets in a leaky dielectric liquid in the presence of an externally applied electric field. A pair of droplets may coalesce or repel each other in the presence of an electric field. Interactions between a pair of drops have been shown to be governed by the ratio ε_r/σ_r, where ε_r and σ_r are the ratios of drop to ambient fluid electric permittivities and conductivities, respectively. When inertia is neglected, the droplets approach each other if $\varepsilon_r/\sigma_r > 1$, whereas droplets repel when $\varepsilon_r/\sigma_r < 1$. However, inclusion of inertia permits interesting transient behaviour, where the droplets may attract due to the electrostatic dipole–dipole attraction even for $\varepsilon_r/\sigma_r < 1$. The approach velocity then is governed by the electrostatic forces and varies as $1/h^4$, where h is the separation distance between the droplets, in contrast to being hydrodynamically driven as predicted in the Stokes flow limit by Baygents *et al.* (*J. Fluid Mech.*, vol. 368, 1998, pp. 359–375). For compound droplets, interactions between droplets are essentially governed by the electrical properties of the outer droplet and the ambient fluid. However, transient dynamics may also result in the breakup of a compound droplet and lead to formation of single droplets.

Key words: emulsions, electrohydrodynamic effects

1. Introduction

An emulsion is a dispersion of drops of one fluid in another. Emulsions are ubiquitous in nature and are extensively used in chemical, coating, food, cosmetics, agricultural and medical industries to achieve products with desired properties. The shelf life of products such as paints, lotions, insecticides, medicines, etc., directly depends on the stability of

† Email address for correspondence: gtom@iisc.ac.in

the emulsions. Usually, emulsions are stabilised using compatible surfactants, also called emulsifiers. While the stability of emulsions is desired in most applications, in some applications, naturally occurring emulsions need to be phase-separated, for example in oil and petroleum industries. Interesting applications utilising the convection currents generated in droplets due to an electric field are emerging. For example, Penkova *et al.* (2006) show that the electric-field-driven flow in a droplet affects the nucleation of protein clusters. Chung & Oliver (1990) showed that electric-field-induced circulation results in enhanced heat transfer in a spherical droplet translating in a dielectric medium. Electric field also affects the wetting characteristics which can be harnessed for various applications in microfluids (see Romero Herreros 2014). Electric field can also be employed to control the size of droplets and bubbles from a nozzle as shown in Notz & Basaran (1999) and Sunder & Tomar (2013). Application of an electric field across an emulsion has been shown to affect the stability of emulsions (Barnes 1994; Kilpatrick 2012; Goodarzi & Zendehboudi 2019). For instance, in the oil refining industry, where the conventional methods for oil dehydration, namely centrifugation, chemical treatment and gravity separation, have shown only limited success, electric field has been recently used effectively for separation of water from emulsified oil (Mhatre & Thaokar 2015). The effect of electric field on a liquid drop has been studied extensively since the time of Rayleigh (1882). Garton & Krasucki (1964) observed in their experiments that bubbles in insulating liquids deform in prolate shapes and showed that with an increase in electric field beyond a critical value, the bubbles can become unstable. Curious flow patterns around a droplet were observed in the experimental investigations of Allan & Mason (1962), Bungenberg de Jong & Hoskam (1941) and O'Konski & Harris (1957), and were explained in the seminal work of Taylor (1966) by incorporating a small but finite conductivity for both the drop and the ambient fluid. Taylor (1966) not only could explain the origin of the circulatory flow, but also showed that the flow generated by the tangential electric stresses at the drop surface can lead to oblate deformation of the droplets, where only prolate drop deformations are expected for perfectly conducting or perfectly dielectric fluids. The leaky dielectric theory, based on these results, is presented in detail in Melcher & Taylor (1969) and has been extensively used since then to explain the behaviour of an isolated droplet in an emulsion. Saville (1997) provides a detailed review of electrohydrodynamics showing the connection between the electrokinetic and the leaky dielectric theories (also see Zholkovskij, Masliyah & Czarnecki 2002).

Subsequent to the deformation predictions in the low-Reynolds-number limit by Taylor (1966), several improvements on the solution have been proposed. Second-order corrections to drop deformation were given by Ajayi (1978), followed by the effect of charge convection on drop deformation as discussed in Feng & Scott (1996), Shutov (2002), Xu & Homsy (2006), Vlahovska (2011), Fernandez (2013) and Lanauze, Walker & Khair (2015). The primary objective of those investigations was to resolve the discrepancy between some of the experimental results of Torza, Cox & Mason (1971) and the theoretical predictions obtained using Taylor's linear theory (Taylor 1966). Taylor's theory is valid only in the limit of small electric capillary number, defined as the ratio of the electric stresses and the capillary pressure, $Ca_E = \varepsilon E_\infty^2 R/\gamma$, where ε is the permittivity of the medium, E_∞ is the strength of the externally applied electric field, R is the radius of the droplet and γ is the surface tension coefficient. Drop deformation at higher Ca_E has also been investigated, mostly numerically (Sherwood 1988; Feng & Scott 1996; Feng 1999; Basaran 2002; Lac & Homsy 2007; Supeene, Koch & Bhattacharjee 2008; Fernandez 2013; Wang, Wang & Qiu 2014; Das & Saintillan 2017*a*), but also theoretically by Ajayi (1978). Stability and breakup of perfectly dielectric droplets under large deformation

have been investigated by Cheng & Chaddock (1984) using energy arguments, and that of charged droplets in air by Brazier-Smith, Jennings & Latham (1971), and for leaky dielectric droplets in a leaky dielectric ambient fluid by Feng & Scott (1996) and Lac & Homsy (2007). Giglio *et al.* (2008) studied the onset of Rayleigh instability in charged conducting microdroplets. The transient dynamics of droplets in electric field has been computationally studied by Sherwood (1988), Esmaeeli & Sharifi (2011), Lanauze, Walker & Khair (2013), Zhang, Zahn & Lin (2013) and Das & Saintillan (2017*b*). The importance of the ratio of charge relaxation time scale to the time scale of other processes such as charge convection due to fluid flow or drop deformation due to local shear has been discussed in Saville (1971), Collins *et al.* (2013) and Lanauze *et al.* (2015). The effect of electric field on compound droplets in double emulsions has also been studied theoretically and experimentally (Gouz & Sadhal 1989; Tsukada *et al.* 1997; Ha & Yang 1999; Behjatian & Esmaeeli 2013; Soni, Juvekar & Naik 2013; Abbasi *et al.* 2017). Most of these studies of compound droplets have focused on the relative deformation of the inner and the outer droplets, and also the possibilities of breakup and release of the inner droplet into the ambient fluid. Gouz & Sadhal (1989) used a bipolar coordinate system to examine various configurations of compound droplets under which a compound droplet is stable in a translational flow for a given set of suitable electrical conductivities and permittivities of the constituent fluids. Ha & Yang (1999) used a domain perturbation method, similar to Taylor (1966), to predict the equilibrium shapes of the inner and the outer droplets and also computed the rheological response of a dilute double emulsion of compound droplets. Recently, Abbasi *et al.* (2017), using a level set method, studied the various modes under which a double emulsion may break up. Abbasi *et al.* (2017) showed that the inner droplet may undergo large oblate deformation whereas the outer droplet undergoes prolate deformation, and thus can lead to bursting of the compound droplet ejecting the inner droplet fluid into the ambient. They showed that, if the inner droplet is not concentrically placed, it may migrate to the outer surface of the compound droplet and be ejected out for certain conductivity and permittivity ratios.

The rheological response of an emulsion has been shown to be altered in the presence of an electric field. Where a considerable effort has been invested in studying the behaviour of isolated droplets in electric fields, which has led to a better understanding of the rheology of dilute emulsions in electric fields (Ha & Yang 1999; Vlahovska 2011; Sengupta, Walker & Khair 2017; Mandal *et al.* 2018), the effect of interactions between the droplets on the rheology and stability of dense emulsions needs to be understood better. There have been some studies of the interaction between droplets and particles suspended in a perfect insulator in the presence of an externally applied electric field (Latham & Roxburgh 1966; Brazier-Smith *et al.* 1971; Arp, Foister & Mason 1980). Due to the relevance to the oil industry and atmospheric science, interactions between conducting droplets suspended in an insulating fluid (such as in water-in-oil systems and water droplets in clouds) in the presence of an electric field have been studied extensively (Pearce 1954; Brazier-Smith 1971; Atten 1993; Zhang, Basaran & Wham 1995; Mhatre & Thaokar 2015) and more recently by Sorgentone *et al.* (2020). A curious phenomenon of electrocoalescence, or rather the phenomenon of non-coalescence, of charged droplets in an electric field has also revived some interest lately in the study of interactions between a pair of droplets in the presence of an electric field (Aryafar & Kavehpour 2007; Ristenpart *et al.* 2009; Anand, Juvekar & Thaokar 2019; Sunder & Tomar 2020). For uncharged droplets in perfectly dielectric fluids, the droplets always attract each other due to dipole–dipole electrostatic interactions. Interactions between a pair of leaky dielectric droplets suspended in a leaky dielectric fluid were first studied theoretically by Sozou (1975). Sozou (1975)

used bispherical harmonics, considering the two drops to be of the same size, to solve for the electric field and the velocity field due to the tangential electric stresses at the drop interface. The key conclusion was that the non-uniformity in the electric field in the region between the droplets increases as the droplets approach distances shorter than two diameters of the droplets and affects the nature of deformation and coalescence dynamics of the droplets. Zhang *et al.* (1995) used a population dynamics approach to study the interaction between droplet pairs, but their study was conducted using perfectly conducting drops dispersed in a perfect dielectric liquid. Using a boundary integral method, Baygents, Rivette & Stone (1998) performed axisymmetric simulations of interactions between two leaky dielectric droplets in leaky dielectric ambient fluid with the axis of symmetry aligned with the electric field. They showed that the hydrodynamic forces dominate the electrostatic forces in the limit of small Reynolds number and dictate the stability of emulsions. An emulsion is rendered unstable when the droplets attract, whereas the emulsion is stable when the droplets repel. Droplets attract each other if the flow due to the electric stresses at the droplet surface is from the poles towards the equator, thus resulting in a velocity field which pulls the droplets together along the axis, with the externally applied electric field direction aligned with the axis. On the other hand, droplets repel each other when the flow is from the equator to the poles. The flow direction can be simply predicted by comparing the drop to ambient electric conductivity and permittivity ratios, σ_r and ε_r, respectively. If $\sigma_r < \varepsilon_r$, flow is from poles to equator and thus droplets are expected to attract, whereas when $\sigma_r > \varepsilon_r$ flow is from the equator to the poles. Baygents *et al.* (1998) showed that the relative velocity between the droplets of perfectly dielectric systems is governed by h^{-4}, where h is the separation distance between the droplets. They showed that, in contrast, for leaky dielectric fluids, droplets attract or repel at a rate proportional to h^{-2} due to the hydrodynamic forces. Tomar *et al.* (2007) proposed a CLSVOF-based method to simulate two-phase leaky dielectric electrohydrodynamics and showed good agreement with the results for drop–drop interaction of Baygents *et al.* (1998). Lin, Skjetne & Carlson (2012) used a phase-field method to simulate interaction between a pair of droplets in the presence of an electric field. The effect of viscosity ratio on the time scale of coalescence was discussed, but the scaling for the relative velocity between the droplets was not examined.

In the present study, we investigate drop–drop interactions in single and double emulsions in the presence of an electric field using a two-phase flow solver based on a volume of fluid method. The scaling for the relative velocity between the interacting droplets is studied first and it is shown that it can vary as h^{-2} or h^{-4} (where h is the centre-to-centre distance between the droplets) depending upon the Reynolds number of the flow generated by the tangential electric stresses. Then, we present simulations for low-viscosity fluids (with the ambient to drop viscosity ratio as one), for which the droplets attract initially but eventually repel each other. For certain electric properties of the drops and the ambient fluid, we show that the droplets attract, but the coalescence phenomenon is delayed due to the slow drainage of the film between the droplets and a drop-pair doublet is formed similar to the particle pairs formed in Arp & Mason (1977), chain of droplets in Holto, Berg & Lundgaard (2009) and cell–cell (vesicle) doublets in Zimmermann & Vienken (1982). These nonlinear effects due to the finite Reynolds number have not been explored before. Finally, we study the behaviour of compound droplets in an electric field and the effect of electric field on the drop–drop interactions between compound droplets.

The paper is organised as follows. The problem definition and numerical scheme used in this study are discussed in § 2. Results and discussions of the simulations of single

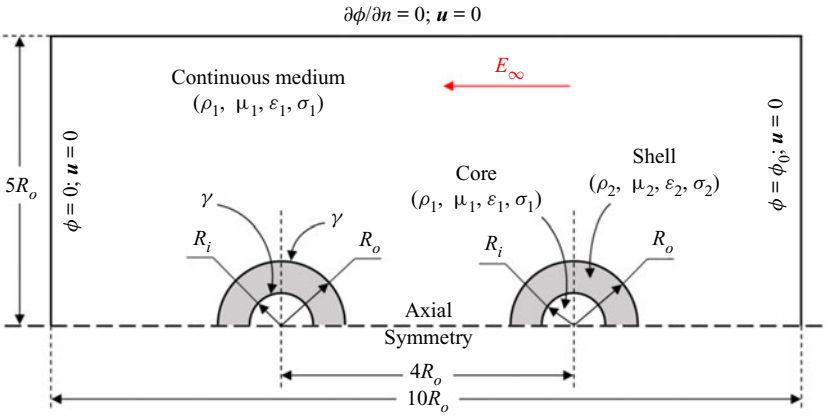

Figure 1. Schematic (not to scale) showing a pair of compound droplets interacting in the presence of an externally applied electric field. The radii of the outer and inner droplets are R_o and R_i, respectively. Various electric, transport and thermodynamic properties are marked in the schematic.

and compound droplets in single and double emulsions, respectively, are presented in § 3. Important conclusions from the study are discussed in § 4.

2. Problem formulation

We study the interaction dynamics of a pair of leaky dielectric single and compound droplets in a leaky dielectric ambient fluid under the influence of an externally applied electric field using an axisymmetric formulation. The initial configuration of the emulsion droplets for the computations is shown in the schematic in figure 1. The dashed line marks the axis of symmetry (along the horizontal direction). The extent of the domain in the radial and axial directions is $5R_o$ and $10R_o$, respectively, where R_o is the radius of the outer shell of the compound droplet (see figure 1). The chosen computational domain is large enough to neglect the effect of the boundary on the dynamics of the droplets at the time scales considered in this study. The initial separation distance between the droplets is $4R_o$. An external electric field is applied along the axial direction and is imposed using $\phi = \phi_0$ as the boundary condition on the right-hand boundary, where ϕ denotes the electric potential (marked in figure 1). The left-hand boundary is electrically grounded using the boundary condition $\phi = 0$. Neumann boundary condition for the electric potential is imposed on the top boundary ($r = 5R_o$), $\partial\phi/\partial r = 0$, where $\partial/\partial r$ denotes the derivative in the radial direction. Symmetry boundary conditions are imposed on the axis of symmetry for the velocity field and the electric potential, and no-slip velocity boundary conditions are imposed on the other boundaries.

We consider the droplets to be neutrally buoyant with densities $\rho_1 = \rho_2$. Here, the properties of the outer fluid are denoted by subscript 1, whereas the fluid constituting the shell of the compound droplet is denoted using the subscript 2 (as marked in figure 1). The properties of the fluid constituting the dispersed phase of the compound droplet are considered to be the same as those of the outer fluid and are denoted by subscript 1. Viscosities of the fluids 1 and 2 are given by μ_1 and μ_2, respectively. Electric permittivities and conductivities are ε_1 and σ_1, respectively, for the ambient fluid and ε_2 and σ_2 for the outer-drop fluid. The two-phase system can be categorised by the following ratios of different properties: $\rho_r = \rho_2/\rho_1$, $\mu_r = \mu_2/\mu_1$, $\varepsilon_r = \varepsilon_2/\varepsilon_1$ and $\sigma_r = \sigma_2/\sigma_1$. For the

simulations presented in this study, we assume $\rho_r = 1$ and $\mu_r = 1$. The fluids involved are assumed to be incompressible and Newtonian, and the surface tension coefficient of the interface between the two fluids is given by $\gamma_{12} = \gamma$. In the following, we discuss the governing equations and the numerical formulation employed for the simulations.

The two-phase system discussed above is governed by the modified incompressible Navier–Stokes equations using the one-fluid formulation as

$$\boldsymbol{\nabla} \cdot \boldsymbol{u} = 0, \tag{2.1}$$

$$\rho(C)\left(\frac{\partial \boldsymbol{u}}{\partial t} + \boldsymbol{\nabla} \cdot \boldsymbol{uu}\right) = -\boldsymbol{\nabla} p + \boldsymbol{\nabla} \cdot [\mu(C)(\boldsymbol{\nabla u} + \boldsymbol{\nabla u}^T)] + \gamma \kappa \boldsymbol{n} \delta_s + \boldsymbol{F}_{el}, \tag{2.2}$$

where $\boldsymbol{u}$ is the velocity field, p is the pressure and the indicator function C is given by the volume fraction that takes a value of zero in fluid 1 and one in fluid 2. The density and viscosity are functions of the volume fraction and are given by $\rho(C) = \rho_2 C + \rho_1(1 - C)$ and $\mu(C) = \mu_2 C + \mu_1(1 - C)$. Surface tension force is modelled as a volumetric force given by $\gamma \kappa \boldsymbol{n} \delta_s$, where γ is the surface tension coefficient, κ is the curvature at the interface, $\boldsymbol{n}$ is the normal vector and δ_s is the smoothed Dirac delta function. Similarly, electric field force $\boldsymbol{F}_{el}$ can be modelled as a volumetric force given by (Melcher & Taylor 1969)

$$\boldsymbol{F}_{el} = -\tfrac{1}{2}(\boldsymbol{E} \cdot \boldsymbol{E})\boldsymbol{\nabla} \varepsilon + q_v \boldsymbol{E}, \tag{2.3}$$

where $\boldsymbol{E}$ is the electric field and q_v is the volumetric free charge. The first term in the above equation is the dielectrophoretic force and the second term is the electrophoretic force arising due to the presence of free charges. The electric force can also be written in terms of the divergence of the Maxwell stress tensor as follows:

$$\boldsymbol{F}_{el} = \boldsymbol{\nabla} \cdot \boldsymbol{T}_e, \tag{2.4}$$

where the Maxwell stress tensor $\boldsymbol{T}_e$ is given by

$$\boldsymbol{T}_e = \varepsilon\left(\boldsymbol{EE} - \frac{E^2}{2}\boldsymbol{I}\right). \tag{2.5}$$

Since the time scales at which the magnetic induction effects become important are significantly smaller than the flow time scales in this study, we ignore the electromagnetic coupling and assume that the electric field $\boldsymbol{E}$ is curl-free ($\boldsymbol{\nabla} \times \boldsymbol{E} = 0$). Thus, we can write $\boldsymbol{E} = -\boldsymbol{\nabla}\phi$. We solve the following Poisson equation with the boundary conditions discussed earlier:

$$\boldsymbol{\nabla} \cdot \varepsilon \boldsymbol{E} = \boldsymbol{\nabla} \cdot (\varepsilon(-\boldsymbol{\nabla}\phi)) = q_v. \tag{2.6}$$

The charge conservation equation is given by

$$\frac{\partial q_v}{\partial t} + \boldsymbol{u} \cdot \boldsymbol{\nabla} q_v + \boldsymbol{\nabla} \cdot \boldsymbol{J} = 0. \tag{2.7}$$

Here, $\boldsymbol{J} = (\sigma \boldsymbol{E})$ is the current density. The electric permittivity and conductivity, in the one-fluid formulation, are given by $\varepsilon = \varepsilon_2 C + \varepsilon_1(1 - C)$ and $\sigma = \sigma_2 C + \sigma_1(1 - C)$, respectively. The evolution of the interface is governed by an advection equation in terms of the volume fraction (C):

$$\frac{\partial C}{\partial t} + \boldsymbol{u} \cdot \boldsymbol{\nabla} C = 0. \tag{2.8}$$

We note that when the electric conductivities of the two fluids are such that the charge relaxation time constants, ε_1/σ_1 and ε_2/σ_2, are small in comparison to the flow time

scales, the charge conservation equation reduces to $\nabla \cdot \boldsymbol{J} = 0$. Thus, the bulk is essentially charge-free and the free charge accumulation only occurs at the interface where there is change in the relaxation time constant. Therefore, both the dielectrophoretic forces and the electrophoretic forces are surface forces acting only at the interface. The surface tension force and the surface electric force are modelled as volumetric forces in the one-fluid formulation using a modified version of the continuum surface force framework proposed by Brackbill, Kothe & Zemach (1992).

The above one-fluid formulation can be shown to impose the following boundary conditions implicitly. Using Gauss's law at the interface yields the jump condition in the normal component of the electric field:

$$\|\varepsilon \boldsymbol{E} \cdot \boldsymbol{n}\| = q_s, \tag{2.9}$$

where $\|\cdot\|$ indicates the jump in the quantity across the interface in the direction of the normal vector $\boldsymbol{n}$. Here, q_s is the surface charge density of free charge and $\boldsymbol{n}$ is the normal at the interface. Since no phase change is involved, we have velocity continuity at the interface:

$$\|\boldsymbol{u} \cdot \boldsymbol{n}\| = 0. \tag{2.10}$$

Normal stress balance condition at the interface yields

$$\|p\| = \gamma\kappa + \|\boldsymbol{n} \cdot \boldsymbol{T}_v \boldsymbol{n}\| + \|\boldsymbol{n} \cdot \boldsymbol{T}_e \boldsymbol{n}\|, \tag{2.11}$$

where $\|p\|$ denotes the jump in pressure, $\gamma\kappa$ is the component of the pressure jump due to surface tension, $\|\boldsymbol{n} \cdot \boldsymbol{T}_v \boldsymbol{n}\|$ is the jump in the normal component of the viscous stress ($\boldsymbol{T}_v = \mu(C)(\nabla \boldsymbol{u} + \nabla \boldsymbol{u}^T)$) across the drop surface and $\|\boldsymbol{n} \cdot \boldsymbol{T}_e \boldsymbol{n}\|$ is the jump in the normal component of the Maxwell stress tensor defined in (2.5). In the absence of any variation in the surface tension coefficient, tangential stress balance is given by

$$\|\boldsymbol{t} \cdot \boldsymbol{T}_v \boldsymbol{n}\| + \|\boldsymbol{t} \cdot \boldsymbol{T}_e \boldsymbol{n}\|. \tag{2.12}$$

Conservation of the surface charge is ensured by accounting for advection of the interface, along with the change in area of the interface due to motion. Thus, surface charge conservation equation is given by

$$\frac{\partial q_s}{\partial t} + \boldsymbol{u} \cdot \nabla_s q_s = q_s \boldsymbol{n} \cdot (\boldsymbol{n} \cdot \nabla)\boldsymbol{u} - \|\sigma \boldsymbol{n} \cdot \boldsymbol{E}\| + \|q_v \boldsymbol{v} \cdot \boldsymbol{n}\|, \tag{2.13}$$

where the term $q_s \boldsymbol{n} \cdot (\boldsymbol{n} \cdot \nabla)\boldsymbol{u}$ accounts for the change in charge density due to the change in the interfacial area. Variation in surface charge density due to the difference in the current density across the interface is given by the term $\|\sigma \boldsymbol{n} \cdot \boldsymbol{E}\|$. The term $\|q_v \boldsymbol{v} \cdot \boldsymbol{n}\|$ corresponds to the transport of charge from the bulk to the interface by the fluid motion near the interface as suggested by (22′) in Saville (1997).

In the one-fluid formulation, we solve a volumetric charge conservation equation which also accounts for the surface charge conservation in a thin diffused layer (over one to three grid cells) at the interface. The efficacy of the one-fluid formulation has been demonstrated in Tomar *et al.* (2007) and López-Herrera, Popinet & Herrada (2011). The algorithm used in the present case is from the latter study which employs a charge conservation approach.

The governing equations for mass, momentum and charge conservation along with the Poisson equation for the electric field potential are solved numerically in the one-fluid formulation. Geometric volume of fluid, coupled with level set method, has been used previously for several electrohydrodynamic problems (see e.g. Tomar *et al.* 2007; Sunder & Tomar 2020). Here, in order to investigate the coalescence outcomes of compound droplets

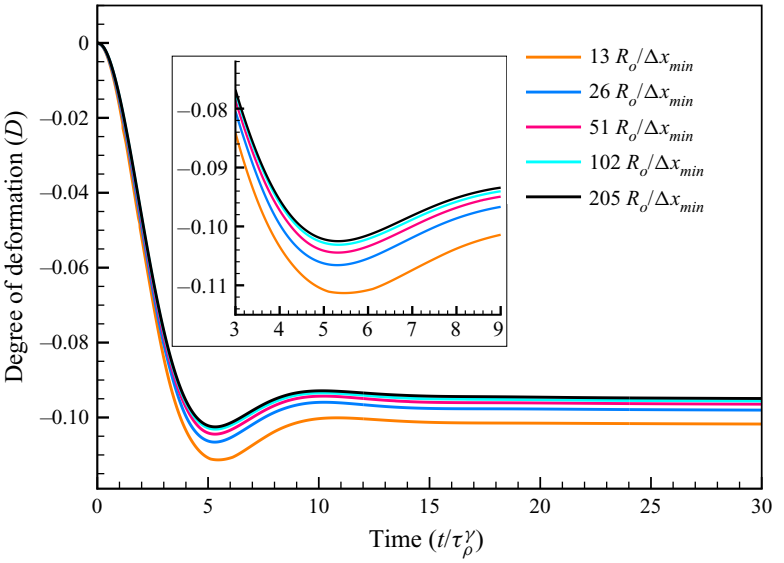

Figure 2. Temporal variation of deformation of the shell under a steady electric field, using five different grid refinements. The parameters considered for the simulations are electric capillary number $Ca_E = 0.2$, $Oh = 1.41$, $\sigma_r = 0.1$, $\varepsilon_r = 2$ and $Re_E = 0.772$.

in electric field, we employ an open source, adaptive mesh refinement (AMR)-based, parallel-flow solver: Basilisk (Popinet 2015). Basilisk, similar to Gerris (Popinet 2003, 2009; Tomar *et al.* 2010), is based on an Oct-Tree AMR. López-Herrera *et al.* (2011) simulated electrohydrodynamics by modifying Gerris and compared the accuracy of the numerical scheme with that of Tomar *et al.* (2007). A similar numerical scheme has been used in Basilisk as well. A geometric volume of fluid method is implemented in Basilisk with the interface approximated by a piecewise linear reconstruction. In Basilisk, normal and curvature at the interface are computed using the height function approach, similar to that in Popinet (2009). Geometric advection of volume of fluid (equation (2.8)) is carried out using a second-order Godunov scheme (Bell, Colella & Glaz 1989) and a balanced-force discretisation, for both electric stresses and surface tension force, is used to minimise spurious currents (Francois *et al.* 2006). A collocated grid discretisation is used and an approximate projection scheme is used to solve the Navier–Stokes equations. Details of the discretisation of the governing equations ((2.2), (2.6), (2.7) and (2.8)) along with detailed validations can be found in Popinet (2015) and López-Herrera *et al.* (2011).

We use AMR to enhance the computational efficiency while maintaining the required accuracy of the simulations. In the present study, we employ AMR using a cost function based on the gradient of the volume fraction, thus using a very fine mesh near the interface while maintaining a relatively coarser mesh elsewhere (see Popinet (2015) for details of the AMR method). To understand the grid requirements for the simulations involving compound droplets presented in this study, we perform a grid independence study. We use the Taylor deformation parameter, defined as $D = (L - B)/(L + B)$, where L is the major axis and B is the minor axis of the deformed compound droplet, to compare numerical convergence with the increase in refinement. We perform simulations using different grid sizes and check the temporal evolution of D as shown in figure 2. The inset shows a zoomed view for minimum value of deformation. The curves corresponding to $R_o/\Delta x_{min} = 102$ and 205 are very close with a maximum difference of 0.6 %. Here, Δx_{min} is the minimum

grid size used in the present study. For the simulations presented in this study, the entire interface is resolved using Δx_{min} and the grid is progressively coarsened away from the droplet. Based on the grid independence study, we use $R_o/\Delta x_{min} = 102$ for the simulations presented in this study.

The following non-dimensional parameters govern the dynamics of droplets due to electrostatic forces and the flow generated by them. Electric capillary number $Ca_E = \mu_1 U_e/\gamma$, where μ_1 is the viscosity of the ambient continuous phase, $\gamma = \gamma_{12}$ is the surface tension coefficient at the interface of fluids 1 and 2 and U_e is the velocity scale defined based on the flow generated by the electric forces. The scaling for velocity generated due to the electric forces can be obtained by balancing viscous stresses with Maxwell stresses at the interface. The scale for the velocity is thus given by $U_e \sim E_\infty^2 \varepsilon_1 R_o/\mu_1$. We note here that the above scaling with an additional factor of $(1 - \tau_e^2/\tau_e^1)\sigma_r/(\sigma_r + 2)^2$ would yield a more appropriate scaling following the solution for velocity given by (27) in Taylor (1966), where $\tau_e^1 = \varepsilon_1/\sigma_1$ and $\tau_e^2 = \varepsilon_2/\sigma_2$ are the charge relaxation time constants for fluid 1 (ambient) and fluid 2 (drop), respectively. Indeed, in our simulations for $\tau_e^1 = \tau_e^2$, no electrohydrodynamic flow is observed (not shown here). Thus, the above scaling for velocity, in some cases, may be an order-of-magnitude different from the observed values. However, for non-dimensionalising velocity, we use U_e defined above as also proposed in Baygents *et al.* (1998), since it allows the delineation of the effects of electrical parameters while comparing results for different values of σ_r and ε_r. Nevertheless, later when we compute scaling for electrostatic and hydrodynamic forces, as well as flow, interface and charge relaxation time scales, we account for the effect of other electrical properties of the fluids on velocity scaling. Using U_e, the electric capillary number can now be written as $Ca_E = E_\infty^2 \varepsilon_1 R_o/\gamma$.

The ratio of the viscous capillary time scale, $\tau_\mu^\gamma = \mu_1 R_o/\gamma$, and the Rayleigh inertial capillary time scale, $\tau_\rho^\gamma = \sqrt{\rho_1 R_o^3/\gamma}$, yields a measure of the role of viscosity in the interfacial dynamics, called the Ohnesorge number: $Oh_1 = \mu_1/\sqrt{\rho_1 R_o \gamma}$ for the ambient fluid; this can be defined similarly for the drop fluid: $Oh_2 = \mu_2/\sqrt{\rho_2 R_o \gamma}$. The Reynolds number, based on U_e, can be defined as $Re = \rho_1 R_o^2 E_\infty^2 \varepsilon_1/\mu_1^2 = Ca_E/Oh_1^2$. An electrical equivalent of the hydrodynamic Reynolds number can also be defined by taking the ratio of charge convection to conduction: $Re_E = U_e \tau_e^1 (1 + \varepsilon_r)/(R_o(1 + \sigma_r))$ as suggested in Feng (1999). Feng (1999) showed that the electric Reynolds number, Re_E, defined above has an effect on the extent of deformation of the droplet.

Using the definition of the electric capillary number Ca_E, we can non-dimensionalise the electric field intensity with $\sim \sqrt{\gamma/\varepsilon_1 R_o}$ (as suggested by Feng (1999)), and thus the non-dimensionalised externally applied electric field intensity can now be written as $E_\infty^* \sim \sqrt{Ca_E}$. Another important parameter requiring attention is the amount of free charge per unit area that develops at the interface: $Q_s \sim 3\varepsilon_1 (1 - \tau_2^e/\tau_1^e) E_\infty/(\sigma_r + 2)$ (computed from an exact solution for a spherical droplet). The ratio of the charge relaxation time constants for the two fluids (τ_2^e/τ_1^e) in the above expression essentially indicates the nature of the charge distribution on the surface of the drop. If the ratio is greater than one, the ambient fluid carries away the charge rapidly and a negative charge develops at the interface (in the northern hemisphere of the droplet with the axis of the droplet aligned with the applied electric field); whereas if the ratio is less than one, the drop fluid supplies positive charge in response to the applied electric field, at a more rapid rate than can be carried away by the ambient fluid, and thus a positive charge accumulates at the surface. The positive or negative charge determines the direction of the tangential stress and thus also the sense of circulation produced by the electrohydrodynamic forces, which in turn determines whether

the nature of the interaction between the droplets is attractive or repelling (see Baygents *et al.* 1998). At low Reynolds number, hydrodynamic viscous forces are stronger and drive the interaction between the droplets, whereas at higher Reynolds numbers, as shown in the next section, the relative velocity during attraction is governed by the electrostatic interaction between the droplets.

In the next section, we discuss the effects of an externally applied electric field on a pair of single and compound droplets.

3. Results and discussion

In this section, we study the interaction dynamics of a pair of droplets, single and compound, suspended in another immiscible fluid under the action of an externally applied electric field. We perform two-dimensional axisymmetric simulations with outer droplet radius R_o and inner droplet radius R_i, as shown in the schematic in figure 1. First, we present results for droplets in a single emulsion ($R_i = 0$). Based on the interaction dynamics of a pair of droplets, we comment on the stability of an emulsion in the presence of an electric field. Subsequently, we discuss interaction dynamics between a pair of compound droplets.

3.1. *Single emulsion in an externally applied electric field*

We validate the numerical model employed in this study by comparing the deformation of a droplet with the theoretical predictions of Taylor (1966) and also previous computational studies (Tomar *et al.* 2007; López-Herrera *et al.* 2011). The size of the domain is the same as that used previously (Tomar *et al.* 2007; López-Herrera *et al.* 2011). All the computations have been performed up to the steady state. Figure 3 shows variation in D with σ_r for $\varepsilon_r = 10$, $Ca_E = 0.18$ and $Oh = 3.16$. We observe that the droplet deforms into an oblate shape ($D < 0$) for low values of σ_r and into a prolate shape ($D > 0$) for higher values of σ_r. In the presence of an electric field, depending on the electrical properties of the two phases, the drop deforms either into an oblate or a prolate shape. Taylor (1966) provided an analytical expression for the deformation of a drop as a function of the fluid properties and the electric field intensity, in the limit of small deformation, as

$$D = \frac{9}{16}\frac{Ca_E}{(2+\sigma_r)^2}\left[1+\sigma_r^2-2\varepsilon_r+\frac{3}{5}(\sigma_r-\varepsilon_r)\frac{2+3\mu_r}{1+\mu_r}\right], \tag{3.1}$$

where $D = (L-B)/(L+B)$ is the Taylor deformation parameter, with L being the length of the droplet along the direction of the electric field and B the width of the droplet in the plane perpendicular to the applied electric field.

The accuracy of Taylor's linear theory has been discussed in several previous studies (Ajayi 1978; Feng 1999), especially in the context of not-so-good agreement with some of the experiments of Torza *et al.* (1971) for low-conductivity fluids. In particular, the deformation of the drop is expected to be proportional to E_∞^2 from the theory, but the experiments of Torza *et al.* (1971) showed only qualitative agreement and the extent of deformation in some cases was over twofold different from the predictions of the theory. Feng (1999) suggested that the possible origin of this discrepancy could be due to the neglect of charge convection in Taylor's theory (see (2.3) in Feng 1999). At low, but finite, electric Reynolds numbers (Re_E), the deviation was shown to be significant especially for very low-conductivity fluids such as silicone and castor oils. In our simulations, we account for charge convection effects. We observe that for small drop deformation there is good agreement between the computational results and Taylor's theory (as shown in

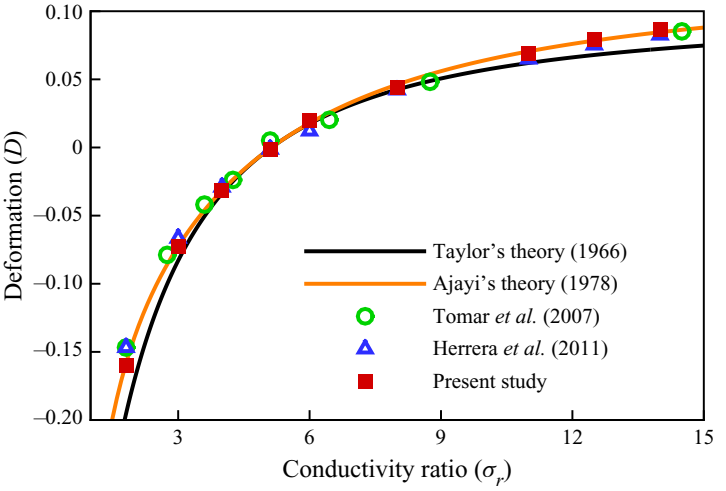

Figure 3. Comparison of deformation (D) of a single droplet with theoretical and computational studies. Other non-dimensional parameters for the computations are $Ca_E = 0.18$, $Oh = 3.16$ and $\varepsilon_r = 10$.

figure 3), and only at larger D is there deviation from the theory essentially due to the breakdown of the assumption of linearity. Comparison with Ajayi's second-order theory shows good agreement with the simulation results. We note that we have focused here on cases where electrical conductivities of the fluids investigated are not as low as those considered by Feng (1999). We will address the physics of the interaction between droplets in very poorly conducting emulsions (e.g. silicone oil droplets in castor oil) in a separate study.

Figure 4 shows the drop shapes and the streamlines of the flow generated by the tangential electric forces. Due to the accumulation of the free charge at the drop interface, a tangential electric force acts at the interface that leads to fluid flow inside the droplet as well as in the ambient fluid, as shown in figure 4 for three different values of σ_r. Other parameters for all three cases shown in figure 4 are $Ca_E = 0.18$, $Oh = Oh_1 = 3.16$ and $\varepsilon_r = 10$. For $\sigma_r = 1.81$ and $\sigma_r = 5.1$, the flow is from poles to equator, resulting in the oblate shape for $\sigma_r = 1.81$ but the droplet remains spherical for $\sigma_r = 5.1$. As indicated by the deformation curve shown in figure 3, a droplet can deform prolately even for $\sigma_r < \varepsilon_r$ (for $\sigma_r > 5.1$ when $\varepsilon_r = 10$ and $\mu_r = 1$) when the electrostatic forces normal to the interface are stronger compared with the hydrodynamics forces. For $\sigma_r = 5.1$, $\varepsilon_r = 10$ and $\mu_r = 1$, the droplet remains spherical. This no-deformation case corresponds to the electrical and fluid properties for which the Maxwell stresses are exactly balanced by the normal viscous stress and the surface tension forces for a spherically shaped droplet. Nevertheless, non-zero tangential electric stresses generate a flow from poles to equator as shown in figure 4(b). The switchover of the flow from poles-to-equator to equator-to-poles occurs when $\sigma_r > \varepsilon_r$ as shown in figure 4(c) for $\sigma_r = 14$ and $\varepsilon_r = 10$. All the computations shown here are in good agreement with the analytical results, as well as with the previous computational studies (Tomar *et al.* 2007; López-Herrera *et al.* 2011).

We now investigate interaction dynamics of two droplets in a single emulsion in the presence of an electric field. The computational domain size for these simulations is $17R_o \times 34R_o$. Charge accumulation at the interface of initially neutrally charged droplets results in the formation of electric dipoles and the droplets interact electrostatically

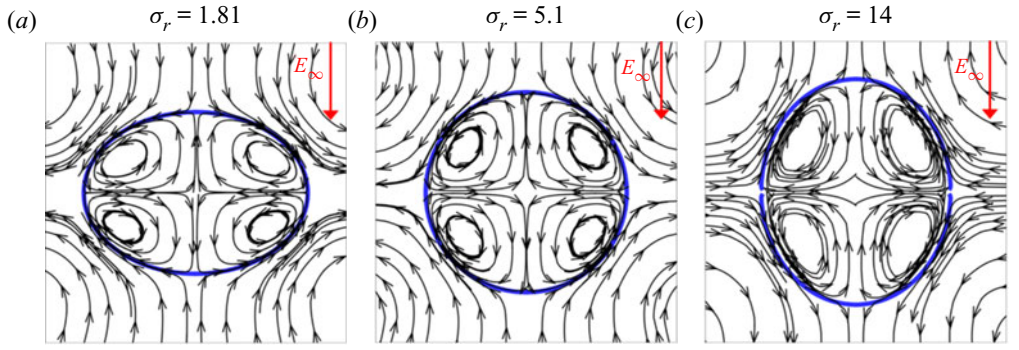

Figure 4. Streamlines and variation in the drop shape for different conductivity ratios. The electric Reynolds number Re_E is (*a*) 2.228, (*b*) 1.027 and (*c*) 0.417. Other parameters are $\varepsilon_r = 10$, $Ca_E = 0.18$ and $Oh = 3.16$.

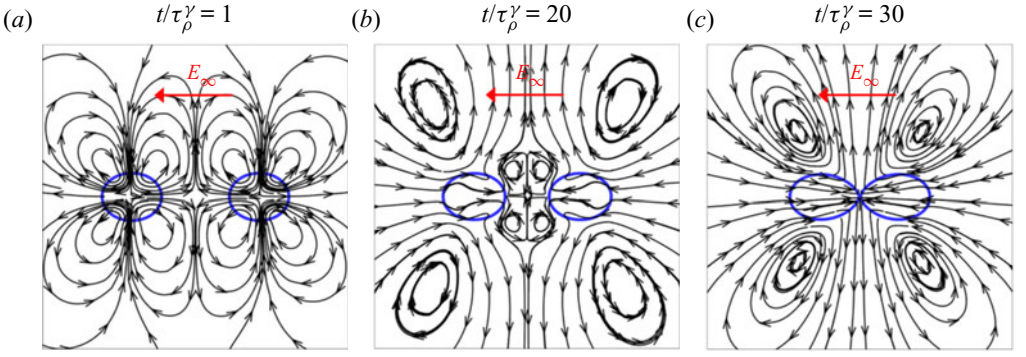

Figure 5. Drop interaction along with the streamline patterns observed at different non-dimensional time (t/τ_ρ^γ) for $\sigma_r = 6$ and $\varepsilon_r = 8$ at $Ca_E = 1.5$ and $Oh = 0.63$. The electric Reynolds number is $Re_E = 4.86$.

through dipole–dipole electrostatic forces. In the large-separation limit, the electrostatic force between the droplets can be shown to be proportional to E_∞^2/h^4, where h is the centre-to-centre spacing between the droplets. On the other hand, flow generated by the electric stress would generate a drag proportional to the relative velocity in the low-Re limit. Thus, the hydrodynamic drag force on one droplet due to the flow generated at the other is proportional to E_∞^2/h^2. However, at higher Re, the hydrodynamic drag is proportional to velocity squared, and thus a drag force proportional to E_∞^4/h^4 should be expected. Simulations presented in this study are for low Ca_E values that correspond to low $Re = Ca_E/Oh^2 \sim O(1)$ and therefore we expect the linear drag law to be valid.

As discussed earlier, the direction of the flow depends upon the sign of $(1 - \tau_e^2/\tau_e^1)$, and therefore is expected to also govern the hydrodynamic interactions between the droplets in an emulsion. Based on the convection currents, the droplets are expected to move towards each other for $\tau_e^2/\tau_e^1 > 1$, or equivalently $\sigma_r < \varepsilon_r$, whereas they will move away from each other for $\tau_e^2/\tau_e^1 < 1$, that is, $\sigma_r > \varepsilon_r$. Here, we present two cases with parameters chosen from Baygents *et al.* (1998) such that the droplets attract in the first case with $\sigma_r = 6$ and $\varepsilon_r = 8$ ($\tau_e^2/\tau_e^1 = \varepsilon_r/\sigma_r = 1.33 > 1$) as shown in figure 5 and therefore are expected to render the emulsion unstable, whereas the droplets repel each other for $\sigma_r = 1.04$ and $\varepsilon_r = 0.2$ ($\tau_e^2/\tau_e^1 \sim 0.2 < 1$) as shown in figure 6, and the electric field is expected to stabilise the emulsion.

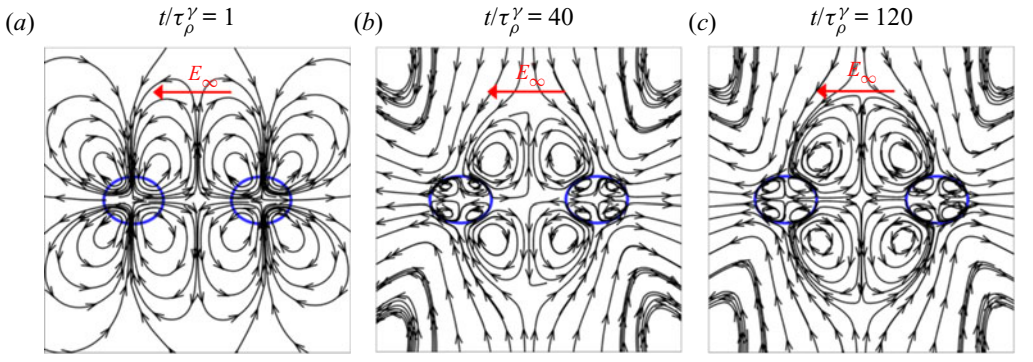

Figure 6. Drop interaction along with the streamline patterns observed at different non-dimensional time (t/τ_ρ^γ) for $\sigma_r = 1.04$ and $\varepsilon_r = 0.2$ at $Ca_E = 1.5$ and $Oh = 0.63$. The electric Reynolds number is $Re_E = 2.223$.

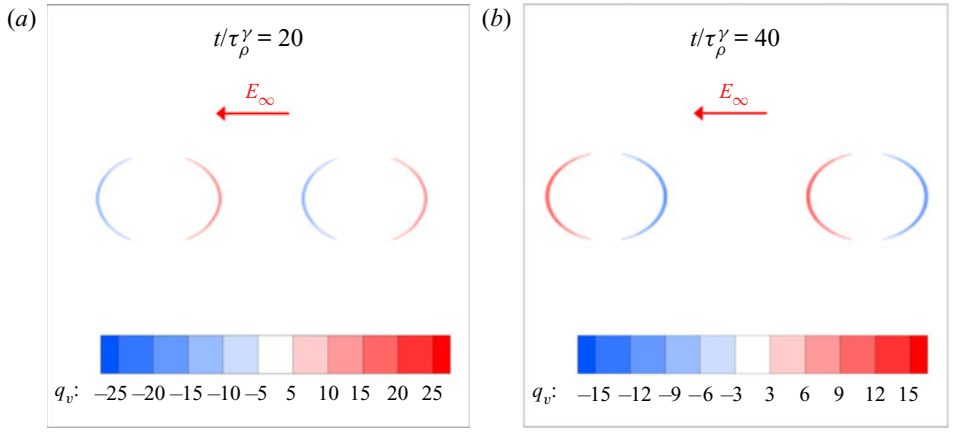

Figure 7. Variation in volumetric charge density (q_v) along the interface for (*a*) $\sigma_r = 6$ and $\varepsilon_r = 8$ ($Re_E = 4.86$) and (*b*) $\sigma_r = 1.04$ and $\varepsilon_r = 0.2$ ($Re_E = 2.223$) at $Ca_E = 1.5$ and $Oh = 0.63$.

In the first case with $\tau_e^2/\tau_e^1 > 1$, charge develops much faster ($t/\tau_\rho^\gamma \sim 0.02$–$0.1 \ll 1$) than the morphological evolution of the droplet $t/\tau_\rho^\gamma \sim 2$. Also, the morphological evolution is much faster than the drop migration time scale $t/\tau_\rho^\gamma \sim 40$. Thus, the drops first deform and subsequently without deforming much, either migrate towards each other or move away depending upon the ratio τ_e^2/τ_e^1. The streamlines for $t/\tau_\rho^\gamma \sim 1$ are similar (see figures 5*a* and 6*a*) for both cases due to the initial prolate deformation. Subsequently, the electric stresses result in a flow which is opposite for the two cases as shown in figures 5(*b*) and 6(*b*). Droplets in figure 5 coalesce, whereas those shown in figure 6 move apart.

Charge distributions for the two cases are presented in figure 7. As discussed earlier, the signs of the charges developing on the drop surfaces are opposite for the two cases shown in figure 7(*a*,*b*). Free charge distribution on the interface for a spherically shaped droplet is given by $Q_s \cos(\theta)$, where the angle θ is measured from the horizontal direction aligned with the applied electric field (as marked in the insets of figure 8). Thus, the charge is maximum at the poles and zero at the equator. For the first case, negative charge develops on the northern hemisphere of the droplet with the axis of the droplet aligned with the electric field, whereas positive charge appears for the second case. Figure 8 shows the

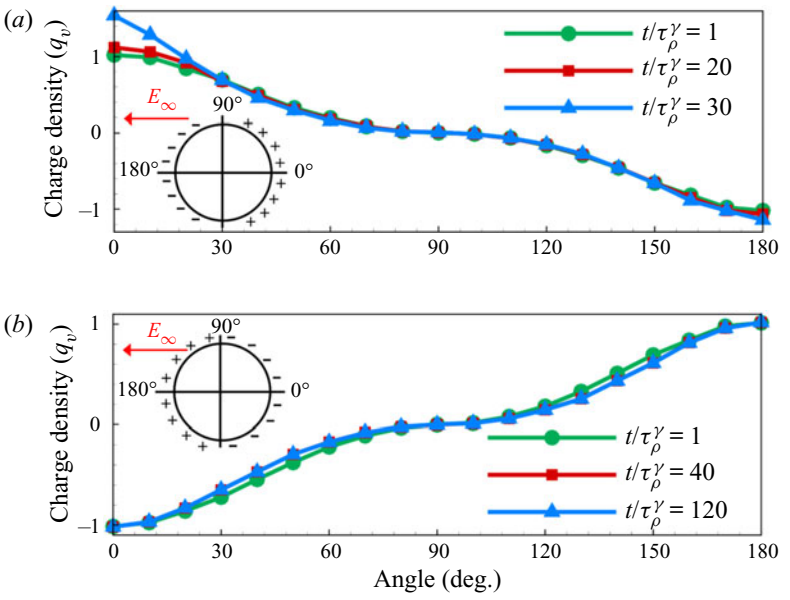

Figure 8. Temporal variation in volumetric charge density (q_v) along the interface and the charge distribution around the interface for (*a*) $\sigma_r = 6$ and $\varepsilon_r = 8$ ($Re_E = 4.86$) and (*b*) $\sigma_r = 1.04$ and $\varepsilon_r = 0.2$ ($Re_E = 2.223$) at $Ca_E = 1.5$ and $Oh = 0.63$.

variation in the charge density on the drop surface for different time instances. Initially when the droplets are far apart, charge develops symmetrically on the northern and the southern hemispheres, similar to the isolated droplet case. However, when the interfaces of the droplets come closer than one diameter, due to non-uniformity in the electric field in the region between the droplets, charge increases in the regions where the droplets face each other.

The dynamics of the droplets shown in the sequence of images in figures 5 and 6 can be understood by comparing the time scales for the different phenomena active during the interaction between the droplets. The time scale of charge accumulation at the drop surface is given by $\tau_e^1/\tau_\rho^\gamma$, which is much shorter due to relatively high conductivities of the fluids considered in the simulations presented in this study. The time scale for the development of the flow due to the tangential electric stresses is given by the time scale for the diffusion of the momentum $\tau_\mu \sim h^2\rho_1/\mu_1$. Thus, $\tau_\mu/\tau_\rho^\gamma \sim h^2/(Oh\,R_o^2)$ yields the time scale for the influence of the electric-stress-driven flow near one drop to reach the other drop. If the droplets are far apart, it will take longer for the flow to develop and thus electrostatic forces may initially influence the droplets before being overtaken by the hydrodynamic forces. Similarly, for low Oh values, even for droplets as close as $h/R_o \sim 5$, $\tau_\mu/\tau_\rho^\gamma$ will be large and the droplets would first respond to the attractive electrostatic forces. Figure 9 demonstrates the above phenomenon for low $Oh = 0.02$ and high $Re_E = 44.131$. The electric Reynolds number is much higher relative to previous cases, thus indicating that the convection is dominant mode of charge transport compared to conduction for the present case, essentially due to the higher ambient velocities for low viscosities (low Oh). For $Oh = 0.63$, droplets repel each other for $\sigma_r = 1.04$ and $\varepsilon_r = 0.2$. However, for $Oh = 0.02$, as shown in figure 9, we observe that the droplets initially attract each other and subsequently when the flow has developed and the hydrodynamic forces are stronger, droplets repel each other.

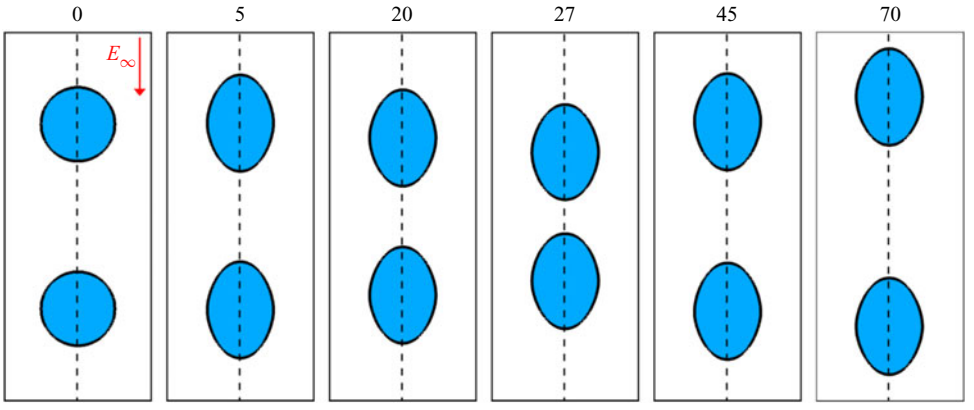

Figure 9. Motion of a pair of droplets for low Ohnesorge number ($Oh = 0.02$) at different non-dimensional time (t/τ_ρ^γ) for $\sigma_r = 1.04$ and $\varepsilon_r = 0.2$ using $Ca_E = 1.5$, $Re_E = 44.131$ and $Oh = 0.02$.

Thus, to determine the nature of the interaction between the droplets, it is not sufficient to look at the ratio of the relaxation time constants (or the direction of the electrically driven convective flow) alone. Baygents *et al.* (1998) also suggested that, in the low-Reynolds-number limit, the droplets interact hydrodynamically when the separation distance is large and they are essentially driven by electrostatic forces when the separation distance is of the order of two droplet diameters. In what follows, we estimate the hydrodynamic and electrohydrodynamic forces, and use the ratio of the forces to determine the nature of the dynamics of a pair of droplets.

Assuming linear drag law for low-Re cases discussed here, we can estimate the net hydrodynamic force on the droplet as (cf. § 4.9 in Batchelor 2000)

$$F_h \sim 4\pi\mu_1 U_e R_o \frac{1 + 3/2\mu_r}{1 + \mu_r}(\boldsymbol{u} - \boldsymbol{v}), \tag{3.2}$$

where $\boldsymbol{v}$ is the velocity of the centre of mass of the droplet, non-dimensionalised by U_e, and the magnitude of the ambient flow velocity $\boldsymbol{u} \sim (R_o/h)^2(\sigma_r - \varepsilon_r)/(\sigma_r + 2)^2$ defines the non-dimensionalised velocity of the ambient fluid. The factor $(\sigma_r - \varepsilon_r)/(\sigma_r + 2)^2$ is the correction for the velocity scale as discussed in the previous section. Electrostatic force between the droplets can be estimated by considering the interactions between the dipoles defined by the sum of the net free and bound charges on the drop surface. For spherical droplets in an electric field, the total charge in the northern hemisphere is given by

$$Q_{net} = 3\pi\varepsilon_0 E_\infty R_o^2 \frac{(\sigma_r - 1)}{(\sigma_r + 2)}, \tag{3.3}$$

where ε_0 is the permittivity of free space. An estimate of the corresponding electrostatic force between the droplets (dipole–dipole interaction), placed at a centre-to-centre separation distance of h, can be obtained as

$$F_e \sim \frac{2Q_{net}^2}{4\pi\varepsilon_1} \frac{R_o^2(R_o^2 - 3h^2)}{h^2(h^2 - R_o^2)^2}. \tag{3.4}$$

The above electrostatic force in the limit of large h results in E_∞^2/h^4 dependence discussed in Baygents *et al.* (1998). The relative strengths of the electrostatic to hydrodynamic forces

can be estimated from the following expression:

$$\frac{F_e}{F_h} \sim \frac{9}{8}\left(\frac{\varepsilon_0}{\varepsilon_1}\right)^2 \frac{(\sigma_r - 1)^2}{(\sigma_r - \varepsilon_r)}\left(\frac{(1+\mu_r)^2}{2+3\mu_r}\right)\frac{1-3(h/R_o)^2}{((h/R_o)^2-1)^2}. \tag{3.5}$$

Thus, from the above expression, the key parameters that govern the relative velocity between the droplets are the ratio of electric conductivities σ_r, initial separation distance between the droplets h/R_o, the ratio of charge relaxation time $\tau_e^2/\tau_e^1 = \varepsilon_r/\sigma_r$ and also the permittivity of the ambient fluid ε_1. Permittivity of the ambient fluid has a detrimental effect on the electrostatic interactions due to dielectric screening effects.

Further, response of the droplets to the hydrodynamic forces is also governed by the relaxation time that accounts for the inertia of the droplet. The relaxation time for a droplet in a flow (cf. Batchelor 2000), τ_R, can be written as

$$\frac{\tau_R}{\tau_\rho^\gamma} = \frac{2\rho_r}{3Oh}\frac{(1+\mu_r)}{(2+3\mu_r)}. \tag{3.6}$$

In the simulations presented in the current study, we have $\rho_r = \mu_r = 1$. Thus, $\tau_R/\tau_\rho^\gamma = 4/(15Oh)$. This indicates that at low Oh, a droplet will not relax to the ambient flow immediately, and thus the droplet may first respond to electrostatic attraction before being driven by the hydrodynamic forces as shown in figure 9. For $Oh \sim 0.02$, we observe that the droplets initially tend to come together but as they approach each other, the flow becomes stronger and they eventually repel each other. The relaxation time constants t_R/t_ρ^γ for $Oh = 0.63$ and $Oh = 0.02$ are 0.42 and 13.33, respectively. Therefore, for $Oh = 0.63$, the droplets quickly relax to the ambient fluid velocity, whereas for $Oh = 0.02$, electrostatic forces initially drive the droplet before the hydrodynamic forces set in. Moreover, as discussed earlier, time for flow development τ_μ/t_ρ^γ ($\sim$1250 for $Oh = 0.02$) is slower for low-viscosity fluids and therefore adds to the effect of slow relaxation time of the droplets. Further, for even lower-viscosity fluids, the droplets can be expected to actually coalesce due to the electrostatic attraction instead of repelling each other due to the hydrodynamic forces (not shown here). Thus, the mutual interaction between the drops of an emulsion is expected to become complex due to the presence of inertial effects in addition to the viscous and electrostatic forces.

For the cases shown in figures 5 and 6, $t_R/t_\rho^\gamma \sim 0.42$ corresponding to a fast deformation of the droplets in response to the electrostatic forces and $\tau_\mu/t_\rho^\gamma \sim 39.68$ which corresponds to the time scale of migration of the droplets. The order of this time scale is in good agreement with the observations from the simulations. For these cases, F_e/F_h is 1.44 and 0.00022, thus clearly suggesting that electrostatic forces are dominant in the first case for $\sigma_r = 6$ and $\varepsilon_r = 8$, whereas for $\sigma_r = 1.04$ and $\varepsilon_r = 0.2$ hydrodynamic forces are dominant. Thus, it is expected that the velocity of attraction will be proportional to $1/h^4$ for the former case and to $1/h^2$ for the latter. We present in figure 10 the variation in the relative centre-of-mass velocity with the separation distance between the droplets on a log–log scale. As expected, relative velocity between the droplets varies as $1/h^4$ for approaching droplets as shown in figure 10(a) and as $1/h^2$ for repelling droplets as shown in figure 10(b).

Other possible interesting behaviour is also observed for a certain set of parameters. For instance, we show that the droplets may approach each other, come close, but not coalesce and instead form a doublet as shown in figure 11. For $\sigma_r = 25$ and $\varepsilon_r = 2$, when the droplets are initially at a separation of $h/R_o = 4$, we obtain $F_e/F_h \sim 4.7$ where the electrostatic forces are attractive but the hydrodynamic forces are repulsive.

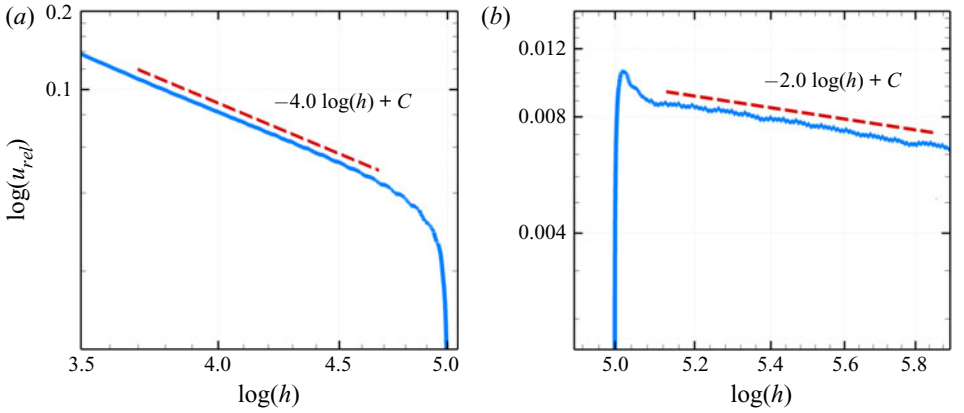

Figure 10. Velocity variation with respect to centre-to-centre distance between the drops for (*a*) $\sigma_r = 6$ and $\varepsilon_r = 8$ ($Re_E = 4.86$) and (*b*) $\sigma_r = 1.04$ and $\varepsilon_r = 0.2$ ($Re_E = 2.223$) at $Ca_E = 1.5$ and $Oh = 0.63$.

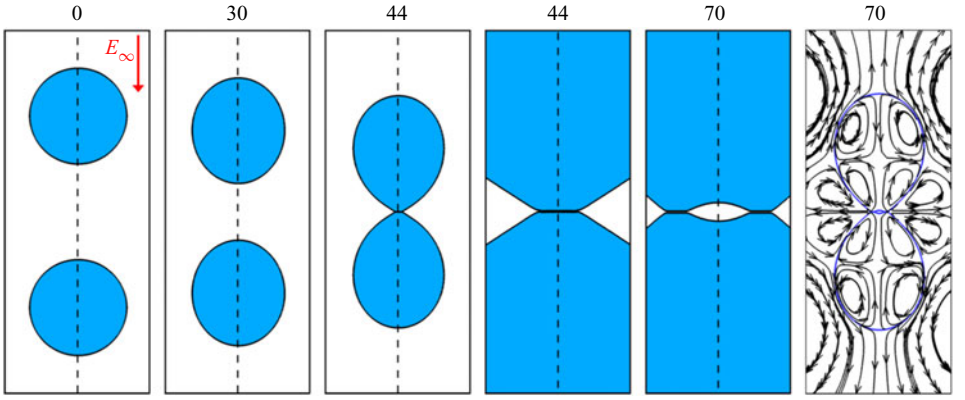

Figure 11. Enlarged view of a pair of non-coalescing droplets at different non-dimensional time (t/τ_ρ^γ) for $\sigma_r = 25$ and $\varepsilon_r = 2$ ($Re_E = 0.092$) at $Ca_E = 0.2$ and $Oh = 0.5$ and the flow patterns around the drop. Also shown are the zoomed-in views (representing the same area) at $t/\tau_\rho^\gamma = 44$ and 70 and streamlines at $t/\tau_\rho^\gamma = 70$.

Since electrostatic forces are stronger, droplets attract but the drainage of the film between the droplets is delayed leading to the formation of a drop–drop doublet the drops of which being separated by a thin film of the ambient fluid as shown in the zoomed-in view in figure 11. The electric Reynolds number $Re_E = 0.092$ is much smaller compared to the other cases presented in this study. A low Re_E indicates much stronger influence of the electrostatic forces compared to the hydrodynamic drag which should have led to coalescence of the droplets. However, due to the nature of the hydrodynamic flow around the droplets, a thin film of the ambient fluid is captured. To resolve the thin film, we use a more refined grid with $\Delta x_{min} = R_0/410$ for the current case. The gap at $t/\tau_\rho^\gamma \sim 44$ is less whereas a dimple forms at the centre of the droplets around $t/\tau_\rho^\gamma \sim 50$ and remains stable at later times, as shown in figure 11 for $t/\tau_\rho^\gamma \sim 70$. We note that once the flat film is fully formed at $t/\tau_\rho^\gamma \sim 50$, further evolution leads to the formation of a dimple essentially due to the drop shape relaxation during which the thin film is pulled together, thus resulting in the formation of the dimple. The minimum thickness of the film is towards the periphery ($\sim 0.0073R_o$) and in the dimple region it is $0.061R_o$. The streamlines shown

in figure 11 indicate that the ambient fluid is driven towards the thin film from the surface of the droplets essentially slowing the drainage of the film. In the simulations, we find that these doublets do not change significantly with time indicating a steady-state behaviour in the time scales of interest. Since we are not incorporating the effect of van der Waals forces, the drainage time is dictated by the slow viscous time scale which in this case is further slowed down due to the ambient fluid flow towards the film. The formation of a dimple in the centre is similar to that observed during coalescence of bubbles or the impact of a droplet on a flat surface. The above phenomenon of non-coalescence and formation of a drop–drop doublet is different from the non-coalescence phenomenon observed for charged droplets, where charged droplets initially approach each other, form a conical neck, exchange charge and then repel each other (Aryafar & Kavehpour 2007; Ristenpart *et al.* 2009; Anand *et al.* 2019; Sunder & Tomar 2020). Although there is no direct mention of the above phenomenon in experimental observations, there is evidence in certain experiments. For example, figures 3 and 4(*a*) of Zimmermann & Vienken (1982) show two vesicles forming doublets during cell–cell fusion in the presence of electric field. Also, figure 5 of Holto *et al.* (2009) suggests the formation of a chain of water droplets in an oil and indicating that the droplets align with the electric field but do not coalesce in spite of being in the immediate neighbourhood of each other. We note that the electric stability of the ambient medium will also play a role in determining the complete physics of interaction, since electric field intensity between the droplets is high which can lead to an electric breakdown leading to a more complex phenomenon involving local heating as discussed in the case of particles by Arp & Mason (1977). We hope that this observation would motivate some careful experiments for drop–drop coalescence in this regime.

3.2. *Double emulsion in an externally applied electric field*

In this section, we first simulate the deformation of a single compound droplet, constituting a double emulsion in an externally applied electric field and compare the results with those of Abbasi *et al.* (2017). As shown in figure 12, the results are in good agreement for the deformation of the constituent droplets. A compound droplet with shell radius R_o and inner droplet radius R_i is suspended in a continuous medium and an externally applied electric field acts along the horizontal direction. The core radius R_i is equal to βR_o. An axisymmetric computational domain of size $(3R_o \times 6R_o)$ is chosen with the compound drop at the centre of the domain. An external electric field is applied such that the right-hand boundary of the domain is considered at a higher potential and the left-hand boundary is grounded as discussed earlier in § 2. The deformation of the outer droplet is similar to that expected for single droplets for low aspect ratios β. For the inner droplet, the deformation will depend on the reduced electric field intensity in the outer droplet and the ratio of the permittivities and conductivities. However, for higher aspect ratios some deviation is expected (see Abbasi *et al.* 2017). The stability of a compound droplet was investigated numerically by Abbasi *et al.* (2017), where it was suggested that if $\varepsilon_r > \sigma_r$, the compound drop is unstable and the inner droplet would exit the outer droplet, whereas if $\varepsilon_r < \sigma_r$ the inner droplet migrates to the centre of the outer droplet. Abbasi *et al.* (2017) also investigated droplet bursting due to excessive deformation of the inner droplet, especially when the aspect ratio β is large. In figure 12(*a*), ε_r is kept constant at 2 and simulations are performed over a range of σ_r varying from 0.1 to 20. When $\sigma_r < \varepsilon_r$, we can observe that both the interfaces experience large deformation. When $\sigma_r > \varepsilon_r$, the magnitude of deformation at both the interfaces decreases which is depicted by the flattening of the curves. In figure 12(*b*), σ_r is kept constant at 2.5 and simulations are

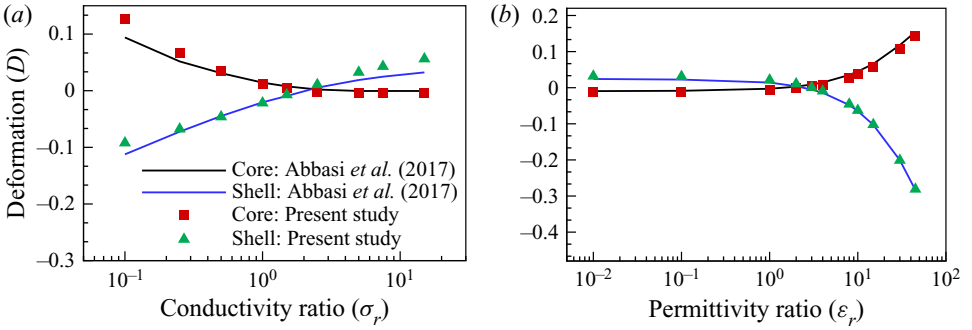

Figure 12. Comparison of deformation of the core and the shell of a compound droplet at $Ca_E = 0.2$ and $Oh = 1.41$ for (*a*) $\varepsilon_r = 2$ and (*b*) $\sigma_r = 2.5$.

performed over a range of ε_r varying from 0.01 to 50. When $\varepsilon_r < \sigma_r$ (for a sufficiently large σ_r for a given ε as discussed previously in the case of an isolated single droplet), the core shows oblate deformation whereas the shell shows prolate deformation. For $\varepsilon_r > \sigma_r$, the shell now shows oblate deformation and the core shows prolate deformation. We note that the deformations of the inner and outer droplets obtained from the simulations presented in this study are in good agreement with those of the simulations of Abbasi *et al.* (2017).

Interactions between compound droplets in a double emulsion can lead to various interesting configurations for different values of σ_r and ε_r. To investigate this, we consider a pair of compound droplets, each with outer radius R_o and inner droplet radius R_i, separated by a centre-to-centre distance of $4R_o$. The shell is three times the size of the core ($\beta = 1/3$). An axisymmetric computational domain of size ($5R_o \times 10R_o$) subjected to an externally applied electric field along the axial direction is considered (see figure 1). The flow parameters used for the simulations are $Ca_E = 0.2$ and $Oh = 0.5$. In figure 13(*a*), for $\sigma_r = 11$ and $\varepsilon_r = 16.5$ ($\sigma_r < \varepsilon_r$), droplets attract and come together and so do the inner droplets, leading to the formation of a single larger compound droplet. The outer droplet (shell) deforms prolately, whereas the deformation of the inner droplet is small. Electric field intensity inside the outer droplet is $\sim 3\boldsymbol{E}_\infty/(\sigma_r + 2)$ and thus, for higher σ_r, it is expected to reduce significantly. The effective Ca_E for the inner droplets is thus much smaller due to the reduced electric field intensity and increased capillary pressure because of smaller radius. Therefore, the inner droplets deform significantly less. Interestingly, during coalescence the inner droplets approach faster than the centroid of the outer droplet. Since the ratio of the electrostatic to hydrodynamic forces is $F_e/F_h \sim 3.42$, electrostatic forces dominate and drive the droplets together, and thus also drag the inner droplets along. Subsequently, hydrodynamic forces on the inner droplets drag them further towards the periphery. This suggests the possibility of the inner droplet escaping the outer droplet as is shown later for $\sigma_r = 10$ and $\varepsilon_r = 27.5$. For $\sigma_r = 3$ and $\varepsilon_r = 0.15$ ($\sigma_r > \varepsilon_r$), shown in figure 13(*b*), the outer droplets move apart at a very slow rate, and therefore do not show much variation in terms of droplet shapes with time for the duration investigated in this study. Further, since $\sigma_r > \varepsilon_r$, the inner droplets are also expected to remain at the centre of the compound droplets. This is in agreement with the observations from the simulations of Abbasi *et al.* (2017), where for $\sigma_r < \varepsilon_r$, an off-centred inner droplet is driven by a flow in the outer droplet from the centre towards the pole, and the inner droplet is ejected out of the outer droplet. On the other hand, if the flow generated in the outer droplet is such that the flow is from the poles towards the centre along the centreline of the droplet (as observed for $\sigma_r > \varepsilon_r$), the inner droplet would be pushed back to the centre of the outer droplet.

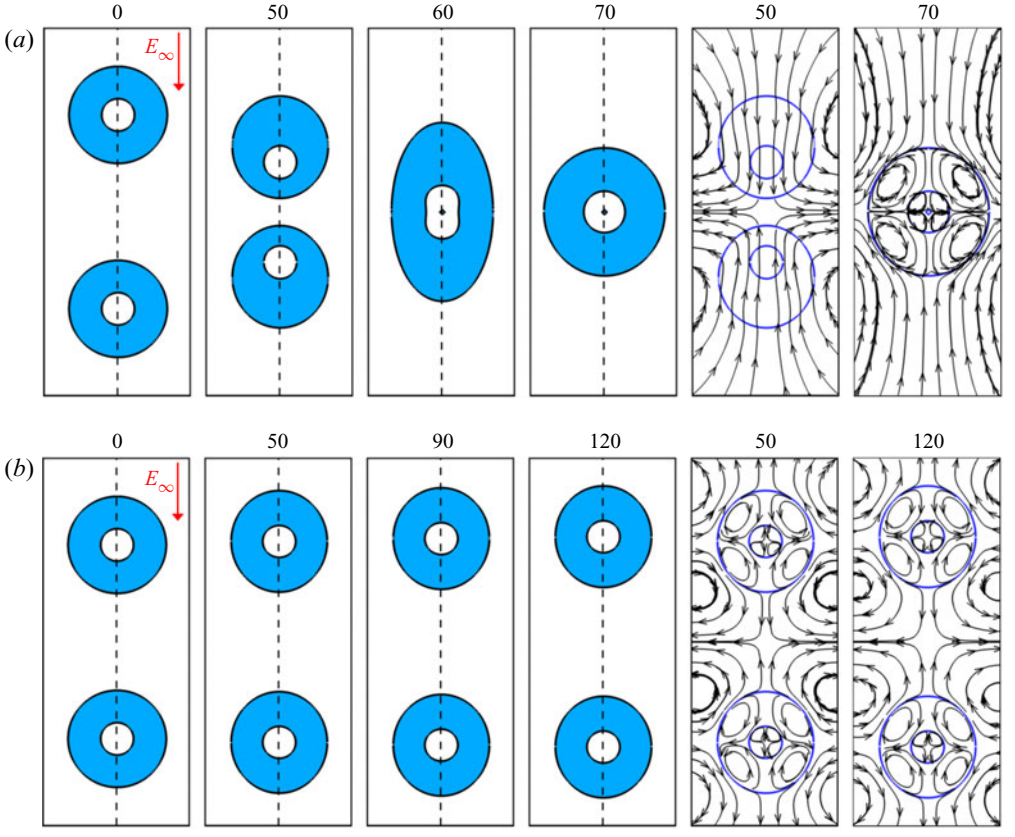

Figure 13. Drop deformation and translation at different non-dimensional time (t/τ_ρ^γ) for (a) $\sigma_r = 11$ and $\varepsilon_r = 16.5$ ($Re_E = 1.167$) and (b) $\sigma_r = 3$ and $\varepsilon_r = 0.15$ ($Re_E = 0.23$) using the flow parameters $Ca_E = 0.2$ and $Oh = 0.5$. We also plot the flow patterns in and around the core and the shell.

Figure 14 shows the variation in the relative velocity of the compound droplets with the separation distance. Oscillations in the relative velocity of the outer droplet as well as for the inner droplets are observed in the repulsion case, as shown in figure 14(b). Since the magnitudes of the velocities are relatively small, the oscillations are more prominently visible in the repulsion case. Since F_e/F_h is 3.42 for $\sigma_r = 10$ and $\varepsilon_r = 27.5$, a scaling of $1/h^4$ is found for the approach velocity of the droplets (see figure 14a); whereas for $\sigma_r = 3$ and $\varepsilon_r = 0.15$, $F_e/F_h \sim 0.26$, and droplets repel each other, governed essentially by the hydrodynamic forces resulting in a relative velocity that decreases as $1/h^2$ as shown in figure 14(b).

For $\sigma_r = 6$ and $\varepsilon_r = 45$, as shown in figure 15(a), the inner droplets escape the compound droplets from the rear ends, as the two compound droplets approach each other. Whereas, for $\sigma_r = 10$ and $\varepsilon_r = 27.5$, the inner droplets are released from the approaching ends of the two compound droplets before they coalesce (see figure 15b), thus resulting in the breakup of the double emulsion into a single emulsion, which as expected for $\sigma_r < \varepsilon_r$ would result in an unstable emulsion in the presence of an electric field. For $\sigma_r = 6$ and $\varepsilon_r = 45$, $F_e/F_h \sim 0.12$; whereas for $\sigma_r = 10$ and $\varepsilon_r = 27.5$, $F_e/F_h \sim 0.87$. Therefore, in the former case, electrostatic forces are much weaker compared to hydrodynamic forces and the small inertial lag of the inner droplet leads to a biased ejection of the inner

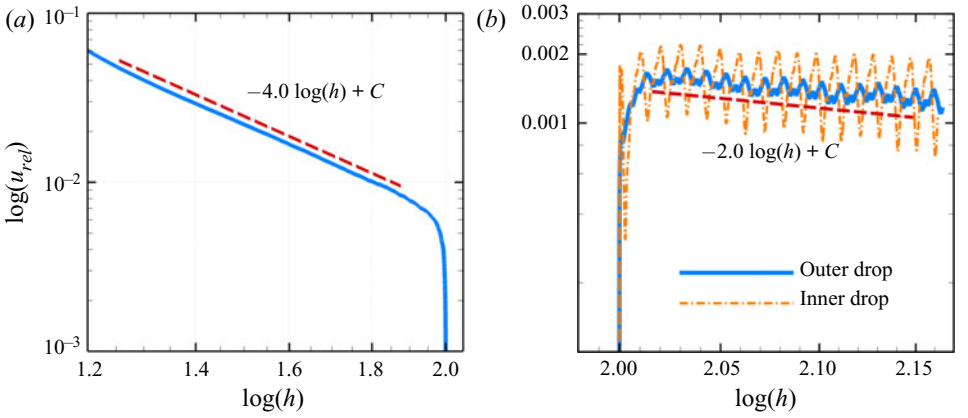

Figure 14. Velocity variation with respect to centre-to-centre distance between the drops for (*a*) $\sigma_r = 11$ and $\varepsilon_r = 16.5$ ($Re_E = 1.167$) and (*b*) $\sigma_r = 3$ and $\varepsilon_r = 0.15$ ($Re_E = 0.23$) at $Ca_E = 0.2$ and $Oh = 0.5$. The motion of the inner core droplet is also depicted using a dash-dotted line.

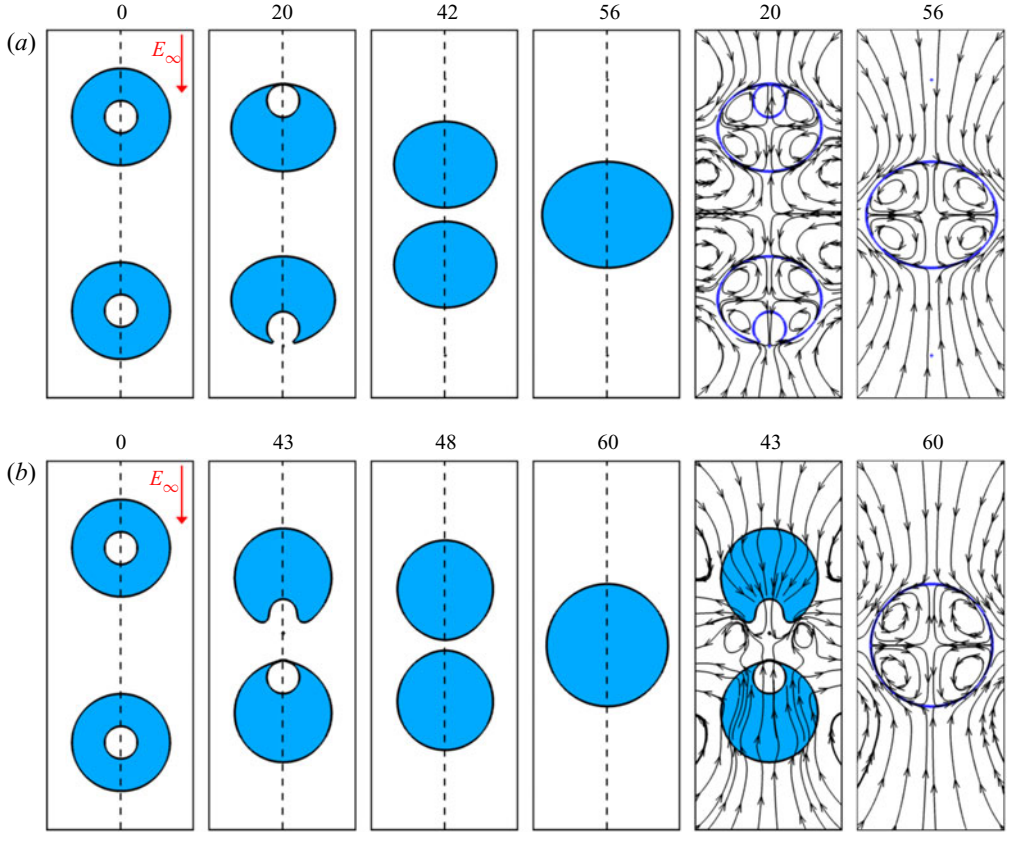

Figure 15. Drop deformation and translation at different non-dimensional time (t/τ_o^γ) for (*a*) $\sigma_r = 6$ and $\varepsilon_r = 45$ ($Re_E = 5.257$) and (*b*) $\sigma_r = 10$ and $\varepsilon_r = 27.5$ ($Re_E = 2.073$) using the flow parameters $Ca_E = 0.2$ and $Oh = 0.5$. We also plot the flow patterns in and around the core and the shell.

droplet from the portion of the periphery of the droplet that faces away from the other compound droplet. On the other hand, for $\sigma_r = 10$ and $\varepsilon_r = 27.5$, electrostatic forces drive the droplets together initially, but are not sufficiently strong as was the case for $\sigma_r = 11$ and $\varepsilon_r = 16.5$, and therefore the inner droplets eject from the portion of the outer droplets facing each other. We note that the hydrodynamic response of the droplets can be weakened by reducing Oh leading to a possible entrapment of the inner droplets even for the case with $\sigma_r = 10$ and $\varepsilon_r = 27.5$.

Finally, we present three cases showing interesting dynamics of the droplets. In the first one, the outer droplets approach each other but do not coalesce but form a drop–drop doublet, as shown in figure 16(a) for $\sigma_r = 25$ and $\varepsilon_r = 2$. As discussed earlier for the single droplets with the same σ_r and ε_r, this interesting physics is due to the strong initial electrostatic attraction and subsequent delay in the drainage of the thin film between the two droplets due to the nature of the flow around the droplets as shown by the streamlines in figure 16(a) for $t/\tau_\rho^\gamma = 100$. Since electrostatic forces are much stronger than hydrodynamic forces as suggested by $F_e/F_h \sim 4.71$, droplets are initially driven together and the flow around the droplets is developed by the motion of the droplets as indicated by the streamlines at $t/\tau_\rho^\gamma = 43$, but the flow lines reverse after the development of the flow generated by the tangential electrical stresses as shown by the streamlines at $t/\tau_\rho^\gamma = 100$. However, for $\sigma_r = 30$ and $\varepsilon_r = 10$, $F_e/F_h \sim 7.9$, indicating an even stronger electric field that drives the droplets to approach each other and eventually coalesce (see figure 16b). These cases clearly indicate that the simple rule depending on the sign of $(\sigma_r - \varepsilon_r)$ for determining the interactions between the droplets is insufficient and the relative strengths of electrostatic and hydrodynamic forces, along with inertial effects governed by Oh, need to be accounted for. Interestingly, the inner droplets for $\sigma_r = 30$ and $\varepsilon_r = 10$ do not coalesce even when simulations are run up to $t/\tau_\rho^\gamma \sim 400$. For $\sigma_r = 7$ and $\varepsilon_r = 10$ shown in figure 16(c), the inner droplets form a configuration similar to that in figure 16(b) but eventually the inner droplets repel (since $\sigma_r < \varepsilon_r$) and are ejected.

4. Summary

In the present study, we have numerically investigated the interaction dynamics of a pair of droplets in a uniform electric field. A leaky dielectric model is employed for this study with the inner and the continuous phase being the same, and the outer shell of the compound droplet being different. We note that the stability of a compound droplet as well the relative motion between a pair of droplets depend essentially on the charge relaxation time constant ratio of the ambient and the outer shell of the compound droplet (τ_e^2/τ_e^1) or equivalently the ratio σ_r/ε_r. This parameter describes the sign of the charge that develops at the droplet interface and thus also the sense of the circulation of the flow generated due to the tangential electric stresses. If the flow is from poles to equator in the ambient fluid, it implies that the flow in the outer shell is from the centre towards the pole. The flow generated in the ambient indicates a hydrodynamic drag on the neighbouring droplet thus driving the two droplets together and making the emulsion unstable. Also, due to the flow inside the outer shell of the compound droplet being from the centre towards the pole, any deviation of the inner droplet from the centre of the compound droplet would result in a hydrodynamic drag that will drive the inner droplet towards the ambient fluid. We show that this simple rule of thumb is not useful when the inertial forces need to be accounted for. Despite the key role played by the hydrodynamic forces governed by the strength of the electric field Ca_E and the ratio of charge relaxation time constants τ_e^2/τ_e^1, we observed that for lower values of Ohnesorge number, Oh, electrostatic dipole–dipole forces can modify certain features of the interaction dynamics. We showed that for low Oh, droplets that are

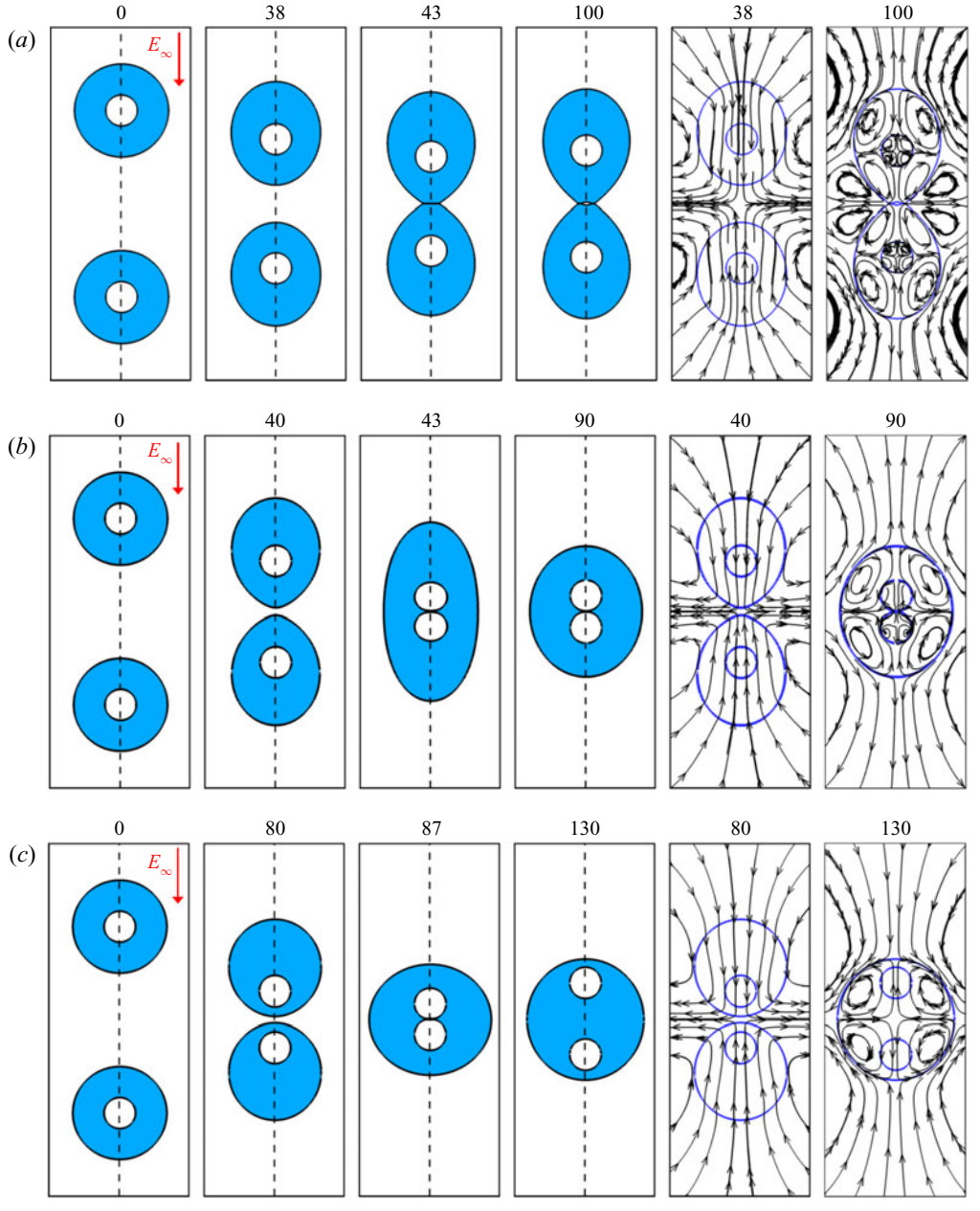

Figure 16. Drop deformation and translation at different non-dimensional time (t/τ_ρ^γ) for (*a*) $\sigma_r = 25$ and $\varepsilon_r = 2$ ($Re_E = 0.092$), (*b*) $\sigma_r = 30$ and $\varepsilon_r = 10$ ($Re_E = 0.284$) and (*c*) $\sigma_r = 7$ and $\varepsilon_r = 10$ ($Re_E = 1.1$) using the flow parameters $Ca_E = 0.2$ and $Oh = 0.5$. We also plot the flow patterns in and around the core and the shell.

expected to repel each other due to the hydrodynamic drag instead approach each other due to the electrostatic interactions. Nevertheless, after initial approach, the droplets eventually repel due to the hydrodynamic forces. This clearly indicates that the *a priori* expectation of the stability of an emulsion in an electric field would require consideration of the relative time scales of electrostatic attraction, charge relaxation and flow time scale.

Moreover, the relative strength of the electrostatic and hydrodynamic forces, given by the ratio F_e/F_h in (3.5), also assists in understanding the interaction dynamics of the droplets. For low F_e/F_h, hydrodynamic forces govern the motion of the droplets and the velocity of approach varies as $1/h^2$, whereas for higher F_e/F_h, electrostatic forces are dominant and the velocity of approach varies as $1/h^4$. We have shown that for certain parameters, where repulsion between the droplets is expected for $\sigma_r/\varepsilon_r > 1$, electrostatic forces can lead to the droplets coming together and coalescing. We believe that this numerical study would motivate some more experiments in regimes that show interesting dynamics of droplets such as the formation of a drop–drop doublet.

Funding. This research received no specific grant from any funding agency, commercial or not-for-profit sectors.

Declaration of interests. The authors report no conflict of interest.

Data availability statement. The corresponding author may be contacted for details of the Basilisk flow solver (open source: http://basilisk.fr/) implementation of the computational work.

Author ORCIDs.
Amaresh Dalal https://orcid.org/0000-0002-4717-2753;
Gaurav Tomar http://orcid.org/0000-0002-5060-4705.

Author contributions. G.T. derived the theory and S.K.D. performed the simulations. All authors contributed equally to analysing data and reaching conclusions, and to writing the paper.

References

Abbasi, M.S., Song, R., Kim, J. & Lee, J. 2017 Electro-hydrodynamic behavior and interface instability of double emulsion droplets under high electric field. *J. Electrostat.* **85**, 11–22.

Ajayi, O.O. 1978 A note on Taylor's electrohydrodynamic theory. *Proc. R. Soc. Lond.* A **364** (1719), 499–507.

Allan, R.S. & Mason, S.G. 1962 Particle behaviour in shear and electric fields. I. Deformation and burst of fluid drops. *Proc. R. Soc. Lond.* A **267** (1328), 45–61.

Anand, V., Juvekar, V.A. & Thaokar, R.M. 2019 Modes of coalescence of aqueous anchored drops in insulating oils under an electric field. *Colloids Surf* A **568**, 294–300.

Arp, P.A., Foister, R.T. & Mason, S.G. 1980 Some electrohydrodynamic effects in fluid dispersions. *Adv. Colloid Interface Sci.* **12** (4), 295–356.

Arp, P.A. & Mason, S.G. 1977 Particle behavior in shear and electric fields. VIII. Interactions of pairs of conducting spheres (theoretical). *Colloid Polym. Sci.* **255**, 566–584.

Aryafar, H. & Kavehpour, P. 2007 Electrocoalescence. *Phys. Fluids* **19** (9), 091107.

Atten, P. 1993 Electrocoalescence of water droplets in an insulating liquid. *J. Electrostat.* **30**, 259–269.

Barnes, H.A. 1994 Rheology of emulsions: a review. *Colloids Surf.* A **91**, 89–95.

Basaran, O.A. 2002 Small-scale free surface flows with breakup: drop formation and emerging applications. *AIChE J.* **48** (9), 1842–1848.

Batchelor, G.K. 2000 *An Introduction to Fluid Dynamics (Cambridge Mathematical Library)*. Cambridge University Press.

Baygents, J.C., Rivette, N.J. & Stone, H.A. 1998 Electrohydrodynamic deformation and interaction of drop pairs. *J. Fluid Mech.* **368**, 359–375.

Behjatian, A. & Esmaeeli, A. 2013 Electrohydrodynamics of a compound drop. *Phys. Rev.* E **88** (3), 033012.

Bell, J.B., Colella, P. & Glaz, H.M. 1989 A second-order projection method for the incompressible Navier–Stokes equations. *J. Comput. Phys.* **85** (2), 257–283.

Brackbill, J.U., Kothe, D.B. & Zemach, C. 1992 A continuum method for modeling surface tension. *J. Comput. Phys.* **100** (2), 335–354.

Brazier-Smith, P.R. 1971 Stability and shape of isolated and pairs of water drops in an electric field. *Phys. Fluids* **14** (1), 1–6.

Brazier-Smith, P.R., Jennings, S.G. & Latham, J. 1971 An investigation of the behaviour of drops and drop-pairs subjected to strong electrical forces. *Proc. R. Soc. Lond.* A **325** (1562), 363–376.

BUNGENBERG DE JONG, H.G. & HOSKAM, E.G. 1941 Motory phenomena in coacervate drops in a diffusion field and in the electric field. *Koninkl. Akad. Wetenschap. Amsterdam* **44**, 1099–1111.

CHENG, K.J. & CHADDOCK, J.B. 1984 Deformation and stability of drops and bubbles in an electric field. *Phys. Lett.* A **106** (1–2), 51–53.

CHUNG, J.N. & OLIVER, D.L.R. 1990 Transient heat transfer in a fluid sphere translating in an electric field. *J. Heat Transfer* **112** (1), 84–91.

COLLINS, R.T., SAMBATH, K., HARRIS, M.T. & BASARAN, O.A. 2013 Universal scaling laws for the disintegration of electrified drops. *Proc. Natl Acad. Sci.* **110** (13), 4905–4910.

DAS, D. & SAINTILLAN, D. 2017*a* Electrohydrodynamics of viscous drops in strong electric fields: numerical simulations. *J. Fluid Mech.* **829**, 127–152.

DAS, D. & SAINTILLAN, D. 2017*b* A nonlinear small-deformation theory for transient droplet electrohydrodynamics. *J. Fluid Mech.* **810**, 225–253.

ESMAEELI, A. & SHARIFI, P. 2011 Transient electrohydrodynamics of a liquid drop. *Phys. Rev.* E **84** (3), 036308.

FENG, J.Q. 1999 Electrohydrodynamic behaviour of a drop subjected to a steady uniform electric field at finite electric reynolds number. *Proc. R. Soc. Lond.* A **455** (1986), 2245–2269.

FENG, J.Q. & SCOTT, T.C. 1996 A computational analysis of electrohydrodynamics of a leaky dielectric drop in an electric field. *J. Fluid Mech.* **311**, 289–326.

FERNANDEZ, A. 2013 Modeling of electroconvective effects on the interaction between electric fields and low conductive drops. In *Fluids Engineering Division Summer Meeting*, vol. 55560, p. V01CT25A004. American Society of Mechanical Engineers.

FRANCOIS, M.M., CUMMINS, S.J., DENDY, E.D., KOTHE, D.B., SICILIAN, J.M. & WILLIAMS, M.W. 2006 A balanced-force algorithm for continuous and sharp interfacial surface tension models within a volume tracking framework. *J. Comput. Phys.* **213** (1), 141–173.

GARTON, C.G. & KRASUCKI, Z. 1964 Bubbles in insulating liquids: stability in an electric field. *Proc. R. Soc. Lond.* A **280** (1381), 211–226.

GIGLIO, E., GERVAIS, B., RANGAMA, J., MANIL, B., HUBER, B.A., DUFT, D., MÜLLER, R., LEISNER, T. & GUET, C. 2008 Shape deformations of surface-charged microdroplets. *Phys. Rev. E* **77** (3), 036319.

GOODARZI, F. & ZENDEHBOUDI, S. 2019 A comprehensive review on emulsions and emulsion stability in chemical and energy industries. *Can. J. Chem. Engng* **97** (1), 281–309.

GOUZ, H.N. & SADHAL, S.S. 1989 Fluid dynamics and stability analysis of a compound droplet in an electric field. *Q. J. Mech. Appl. Maths* **42** (1), 65–83.

HA, J.-W. & YANG, S.-M. 1999 Fluid dynamics of a double emulsion droplet in an electric field. *Phys. Fluids* **11** (5), 1029–1041.

HOLTO, J., BERG, G. & LUNDGAARD, L.E. 2009 Electrocoalescence of drops in a water-in-oil emulsion. In *2009 IEEE Conference on Electrical Insulation and Dielectric Phenomena*, pp. 196–199. IEEE.

KILPATRICK, P.K. 2012 Water-in-crude oil emulsion stabilization: review and unanswered questions. *Energy Fuels* **26** (7), 4017–4026.

LAC, E. & HOMSY, G.M. 2007 Axisymmetric deformation and stability of a viscous drop in a steady electric field. *J. Fluid Mech.* **590**, 239–264.

LANAUZE, J.A., WALKER, L.M. & KHAIR, A.S. 2013 The influence of inertia and charge relaxation on electrohydrodynamic drop deformation. *Phys. Fluids* **25** (11), 112101.

LANAUZE, J.A., WALKER, L.M. & KHAIR, A.S. 2015 Nonlinear electrohydrodynamics of slightly deformed oblate drops. *J. Fluid Mech.* **774**, 245–266.

LATHAM, J. & ROXBURGH, I.W. 1966 Disintegration of pairs of water drops in an electric field. *Proc. R. Soc. Lond.* A **295** (1440), 84–97.

LIN, Y., SKJETNE, P. & CARLSON, A. 2012 A phase field model for multiphase electro-hydrodynamic flow. *Intl J. Multiphase Flow* **45**, 1–11.

LÓPEZ-HERRERA, J.M., POPINET, S. & HERRADA, M.A. 2011 A charge-conservative approach for simulating electrohydrodynamic two-phase flows using volume-of-fluid. *J. Comput. Phys.* **230** (5), 1939–1955.

MANDAL, S., SINHA, S., BANDOPADHYAY, A. & CHAKRABORTY, S. 2018 Drop deformation and emulsion rheology under the combined influence of uniform electric field and linear flow. *J. Fluid Mech.* **841**, 408.

MELCHER, J.R. & TAYLOR, G.I. 1969 Electrohydrodynamics: a review of the role of interfacial shear stresses. *Annu. Rev. Fluid Mech.* **1** (1), 111–146.

MHATRE, S. & THAOKAR, R. 2015 Electrocoalescence in non-uniform electric fields: an experimental study. *Chem. Engng Process* **96**, 28–38.

NOTZ, P.K. & BASARAN, O.A. 1999 Dynamics of drop formation in an electric field. *J. Colloid Interface Sci.* **213** (1), 218–237.

O'Konski, C.T. & Harris, F.E. 1957 Electric free energy and the deformation of droplets in electrically conducting systems. *J. Phys. Chem.* **61** (9), 1172–1174.
Pearce, C.A.R. 1954 The mechanism of the resolution of water-in-oil emulsions by electrical treatment. *Br. J. Appl. Phys.* **5** (4), 136–143.
Penkova, A., Pan, W., Hodjaoglu, F. & Vekilov, P.G. 2006 Nucleation of protein crystals under the influence of solution shear flow. *Ann. N.Y. Acad. Sci.* **1077** (1), 214–231.
Popinet, S. 2003 Gerris: a tree-based adaptive solver for the incompressible euler equations in complex geometries. *J. Comput. Phys.* **190** (2), 572–600.
Popinet, S. 2009 An accurate adaptive solver for surface-tension-driven interfacial flows. *J. Comput. Phys.* **228** (16), 5838–5866.
Popinet, S. 2015 A quadtree-adaptive multigrid solver for the serre–green–naghdi equations. *J. Comput. Phys.* **302**, 336–358.
Rayleigh, L. 1882 XX. on the equilibrium of liquid conducting masses charged with electricity. *Lond. Edinb. Dubl Philos. Mag. J. Sci.* **14** (87), 184–186.
Ristenpart, W.D., Bird, J.C., Belmonte, A., Dollar, F. & Stone, H.A. 2009 Non-coalescence of oppositely charged drops. *Nature* **461** (7262), 377–380.
Romero Herreros, N. 2014 Experimental study of the influence of an electric field on the shape of a droplet. Master's thesis, Universitat Politècnica de Catalunya.
Saville, D.A. 1971 Electrohydrodynamic stability: effects of charge relaxation at the interface of a liquid jet. *J. Fluid Mech.* **48** (4), 815–827.
Saville, D.A. 1997 Electrohydrodynamics: the Taylor–Melcher leaky dielectric model. *Annu. Rev. Fluid Mech.* **29** (1), 27–64.
Sengupta, R., Walker, L.M. & Khair, A.S. 2017 The role of surface charge convection in the electrohydrodynamics and breakup of prolate drops. *J. Fluid Mech.* **833**, 29–53.
Sherwood, J.D. 1988 Breakup of fluid droplets in electric and magnetic fields. *J. Fluid Mech.* **188**, 133–146.
Shutov, A.A. 2002 The shape of a drop in a constant electric field. *Tech. Phys.* **47** (12), 1501–1508.
Soni, P., Juvekar, V.A. & Naik, V.M. 2013 Investigation on dynamics of double emulsion droplet in a uniform electric field. *J. Electrostat.* **71** (3), 471–477.
Sorgentone, C., Kach, J.I., Khair, A.S., Walker, L.M. & Vlahovska, P.M. 2020 Numerical and asymptotic analysis of the three-dimensional electrohydrodynamic interactions of drop pairs. arXiv:2004.05493.
Sozou, C. 1975 Electrohydrodynamics of a pair of liquid drops. *J. Fluid Mech.* **67** (2), 339–348.
Sunder, S. & Tomar, G. 2013 Numerical simulations of bubble formation from submerged needles under non-uniform direct current electric field. *Phys. Fluids* **25** (10), 102104.
Sunder, S. & Tomar, G. 2020 Numerical investigation of a conducting drop's interaction with a conducting liquid pool under an external electric field. *Eur. J. Mech.* B/*Fluids* **81**, 114–123.
Supeene, G., Koch, C.R. & Bhattacharjee, S. 2008 Deformation of a droplet in an electric field: nonlinear transient response in perfect and leaky dielectric media. *J. Colloid Interface Sci.* **318** (2), 463–476.
Taylor, G.I. 1966 Studies in electrohydrodynamics. I. The circulation produced in a drop by an electric field. *Proc. R. Soc. Lond.* A **291** (1425), 159–166.
Tomar, G., Fuster, D., Zaleski, S. & Popinet, S. 2010 Multiscale simulations of primary atomization. *Comput. Fluids* **39** (10), 1864–1874.
Tomar, G., Gerlach, D., Biswas, G., Alleborn, N., Sharma, A., Durst, F., Welch, S.W.J. & Delgado, A. 2007 Two-phase electrohydrodynamic simulations using a volume-of-fluid approach. *J. Comput. Phys.* **227** (2), 1267–1285.
Torza, S., Cox, R.G. & Mason, S.G. 1971 Electrohydrodynamic deformation and bursts of liquid drops. *Philos. Trans. R. Soc. Lond.* A **269** (1198), 295–319.
Tsukada, T., Mayama, J., Sato, M. & Hozawa, M. 1997 Theoretical and experimental studies on the behavior of a compound drop under a uniform dc electric field. *J. Chem. Engng Japan* **30** (2), 215–222.
Vlahovska, P.M. 2011 On the rheology of a dilute emulsion in a uniform electric field. *J. Fluid Mech.* **670**, 481–503.
Wang, J., Wang, B. & Qiu, H. 2014 Coalescence and breakup of oppositely charged droplets. *Sci. Rep.* **4**, 7123.
Xu, X. & Homsy, G.M. 2006 The settling velocity and shape distortion of drops in a uniform electric field. *J. Fluid Mech.* **564**, 395–414.
Zhang, J., Zahn, J.D. & Lin, H. 2013 Transient solution for droplet deformation under electric fields. *Phys. Rev.* E **87** (4), 043008.

ZHANG, X., BASARAN, O.A. & WHAM, R.M. 1995 Theoretical prediction of electric field-enhanced coalescence of spherical drops. *AIChE J.* **41** (7), 1629–1639.

ZHOLKOVSKIJ, E.K., MASLIYAH, J.H. & CZARNECKI, J. 2002 An electrokinetic model of drop deformation in an electric field. *J. Fluid Mech.* **472**, 1–27.

ZIMMERMANN, U. & VIENKEN, J. 1982 Electric field-induced cell-to-cell fusion. *J. Membr. Biol.* **67** (1), 165–182.